Tracing the formation of the Milky Way through ultra metal-poor stars

Federico Sestito, Nicolas Longeard, Nicolas Martin, Else Starkenburg, Morgan Fouesneau, Jonay González hernández, Anke Arentsen, Rodrigo Ibata, David Aguado, Raymond Carlberg, et al.

Monthly Notices
of the
ROYAL ASTRONOMICAL SOCIETY

MNRAS **484,** 2166–2180 (2019)
Advance Access publication 2019 January 9

doi:10.1093/mnras/stz043

Tracing the formation of the Milky Way through ultra metal-poor stars

Federico Sestito,[1,2]★ Nicolas Longeard,[1] Nicolas F. Martin,[1,3] Else Starkenburg,[2] Morgan Fouesneau,[3] Jonay I. González Hernández,[4,5] Anke Arentsen,[2] Rodrigo Ibata,[1] David S. Aguado,[6] Raymond G. Carlberg,[7] Pascale Jablonka,[8,9] Julio F. Navarro,[10] Eline Tolstoy[11] and Kim A. Venn[10]

[1]*Observatoire astronomique de Strasbourg, CNRS, UMR 7550, F-67000 Strasbourg, France*
[2]*Leibniz Institute for Astrophysics Potsdam (AIP), An der Sternwarte 16, D-14482 Potsdam, Germany*
[3]*Max-Planck-Institut für Astronomie, Königstuhl 17, D-69117 Heidelberg, Germany*
[4]*Instituto de Astrofisica de Canarias, Vía Láctea, E-38205 La Laguna, Spain*
[5]*Departamento de Astrofísica, Universidad de La Laguna, Tenerife, E-38206 La Laguna, Spain*
[6]*Institute of Astronomy, University of Cambridge, Madingley Road, CB3 0HA Cambridge, UK*
[7]*Department of Astronomy and Astrophysics, University of Toronto, Toronto, ON M5S 3H4, Canada*
[8]*GEPI, Observatoire de Paris, Université PSL, CNRS, Place Jules Janssen, F-92190 Meudon, France*
[9]*Institute of Physics, Laboratoire d'astrophysique, École Polytechnique Fédérale de Lausanne (EPFL), Observatoire, CH-1290 Versoix, Switzerland*
[10]*Department of Physics and Astronomy, University of Victoria, PO Box 3055, STN CSC, Victoria BC V8W 3P6, Canada*
[11]*Kapteyn Astronomical Institute, University of Groningen, Landleven 12, NL-9747AD Groningen, the Netherlands*

Accepted 2018 December 24. Received 2018 December 20; in original form 2018 November 7

ABSTRACT

We use *Gaia DR2* astrometric and photometric data, published radial velocities and MESA models to infer distances, orbits, surface gravities, and effective temperatures for all ultra metal-poor stars ([Fe/H] < -4.0 dex) available in the literature. Assuming that these stars are old (> 11 Gyr) and that they are expected to belong to the Milky Way halo, we find that these 42 stars (18 dwarf stars and 24 giants or sub-giants) are currently within $\sim$20 kpc of the Sun and that they map a wide variety of orbits. A large fraction of those stars remains confined to the inner parts of the halo and was likely formed or accreted early on in the history of the Milky Way, while others have larger apocentres (> 30 kpc), hinting at later accretion from dwarf galaxies. Of particular interest, we find evidence that a significant fraction of all known UMP stars ($\sim$26 per cent) are on prograde orbits confined within 3 kpc of the Milky Way plane ($J_z < 100$ km s^{-1} kpc). One intriguing interpretation is that these stars belonged to the massive building block(s) of the proto-Milky Way that formed the backbone of the Milky Way disc. Alternatively, they might have formed in the early disc and have been dynamically heated, or have been brought into the Milky Way by one or more accretion events whose orbit was dragged into the plane by dynamical friction before disruption. The combination of the exquisite *Gaia DR2* data and surveys of the very metal-poor sky opens an exciting era in which we can trace the very early formation of the Milky Way.

Key words: stars: distances – Galaxy: abundances – Galaxy: disc – Galaxy: evolution – Galaxy: formation – Galaxy: halo.

1 INTRODUCTION

Ultra metal-poor (UMP) stars, defined to have [Fe/H][1] < -4 dex (Beers & Christlieb 2005), are extremely rare objects located mainly in the Milky Way (MW) halo. Because they are ultra metal-poor, also relative to their neighbourhood, it is assumed that they formed from relative pristine gas shortly after the big bang (e.g. Freeman & Bland-Hawthorn 2002). As such, they belong to the earliest generations of stars formed in the Universe (Karlsson, Bromm & Bland-Hawthorn 2013). Because they are old, observable UMPs must be low-mass stars, however the minimum metallicity at which low-mass stars can form is still an open question (see Greif 2015; and references therein). The search for, and study of, stars with the lowest metallicities are therefore important topics to answer

★ E-mail: federico.sestito@astro.unistra.fr

[1] [Fe/H] $= \log(N_{Fe}/N_H)_\star - \log(N_{Fe}/N_H)_\odot$, with N_X= the number density of element X.

questions on the masses of the first generation of stars and the universality of the initial mass function (IMF), as well as on the early formation stages of galaxies and the first supernovae (e.g. Frebel & Norris 2015; and references therein). Careful studies over many decades have allowed us to build up a catalogue of 42 UMP stars throughout the Galaxy. Many of these stars were discovered in survey programs that were or are dedicated to finding metal-poor stars using some special pre-selection through prism techniques (e.g. the HK and HES surveys; Beers, Preston & Shectman 1985; Christlieb, Wisotzki & Graßhoff 2002) or narrow-band photometry (such as for instance the SkyMapper and Pristine survey programmes; Starkenburg et al. 2017a; Wolf et al. 2018). Others were discovered in blind but very large spectroscopic surveys such as SDSS/SEGUE/BOSS (York et al. 2000; Yanny et al. 2009; Eisenstein et al. 2011) or LAMOST (Cui et al. 2012).

From the analysis of cosmological simulations, predictions can be made for the present-day distribution of such stars in MW-like galaxies. Since these predictions have been shown to be influenced by the physics implemented in these simulations, we can use the present-day distribution to constrain the physical processes of early star formation. For instance, a comparison between the simulations of Starkenburg et al. (2017b) and El-Badry et al. (2018) indicates a clear sensitivity of the present-day distribution on the conditions applied for star formation and the modelling of the ISM.

In an effort to refine the comparison with models and unveil the phase-space properties of these rare stars, we combine the exquisite *Gaia DR2* astrometry and photometry (Gaia Collaboration 2018) with models of UMP stars (MESA isochrones and luminosity functions; Paxton et al. 2011; Choi et al. 2016; Dotter 2016; waps.cfa.harvard.edu/MIST) to infer the distance, stellar properties, and orbits of all 42 known UMP stars.

This paper is organized as follows: Section 2 explains how we put our sample together while Section 3 presents our statistical framework to infer the distance, effective temperature, surface gravity, and orbit of each star in the sample using the *Gaia DR2* information (parallax, proper motion, and G, BP, and RP photometry). The results for the full sample are presented in Section 4 and we discuss the implications of the derived orbits in Section 5 before concluding in Section 6. We refer readers who are interested in the results for individual stars to Appendix A (available Online), in which each star is discussed separately.

2 DATA

We compile the list of all known ultra metal-poor ([Fe/H] < -4.0 dex), hyper metal-poor ([Fe/H] < -5.0 dex), and mega metal-poor ([Fe/H] < -6.0 dex) stars from the literature building from the Joint Institute of Nuclear Astrophysics catalogue (Abohalima & Frebel 2017), supplemented by all relevant discoveries. The literature properties for these stars are listed in Table 1. We crossmatch this list with the *Gaia DR2* catalogue[2] (Gaia Collaboration 2018) in order to obtain the stars' photometric and astrometric information. This is listed in Table 2.

Some stars were studied in more than one literary source, with different methods involving 1D or 3D models and considering the stellar atmosphere at Local Thermodynamic Equilibrium (LTE) or non-LTE, leading to dissimilar results on metallicity and stellar parameters. In this paper, when multiple results are available, we report in Table 1 preferentially results including 3D stellar atmosphere and/or involving non-LTE modelling. If all results are in 1D LTE, we favour the most recent results.

When the UMP stars are recognized to be in binary systems and the orbital parameters are known (see Table 1), the reported radial velocity is the systemic value that is corrected for the binary orbital motion around the centre of mass.

Assuming that all stars in our sample are distant, we consider that all the extinction is in the foreground. Therefore, all stars are dereddened using the Schlegel, Finkbeiner & Davis (1998) extinction map as listed in Table 1 and the Marigo et al. (2008) coefficients for the Gaia filters based on Evans et al. (2018), i.e.

$$G_0 = G - 2.664E(B-V), \tag{1}$$

$$BP_0 = BP - 3.311E(B-V), \tag{2}$$

$$RP_0 = RP - 2.021E(B-V). \tag{3}$$

Extinction values remain small in most cases (Table 1).

We assume that the distance between the Sun and the Galactic centre is 8.0 kpc, that the Local Standard of Rest circular velocity is $V_c = 239\,\mathrm{km\,s^{-1}}$, and that the peculiar motion of the Sun is ($U_0 = 11.10\,\mathrm{km\,s^{-1}}$, $V_0 + V_c = 251.24\,\mathrm{km\,s^{-1}}$, $W_0 = 7.25\,\mathrm{km\,s^{-1}}$) as described in Schönrich, Binney & Dehnen (2010).

3 INFERRING THE PROPERTIES OF STARS IN THE UMP SAMPLE

3.1 Distance inference

It is ill advised to calculate the distance to a star by simply inverting the parallax measurement (Bailer-Jones 2015), especially for large relative measurement uncertainties (e.g. $\delta\varpi/\varpi > 0.2$) and negative parallaxes. Therefore, we infer the probability distribution function (PDF) of the heliocentric distance to a star by combining its photometric and astrometric data with a sensible MW stellar density prior. Following Bayes' rule (Sharma 2017), the posterior probability of having a star at a certain distance given its observables $\boldsymbol{\Theta}$ (e.g. photometry, metallicity, parallax) and a model $\mathcal{M}$ is characterized by its likelihood $\mathcal{L}(\boldsymbol{\Theta}|\mathcal{M})$ and the prior $\mathcal{P}(\mathcal{M})$. The likelihood gives the probability of the set of observables $\boldsymbol{\Theta}$ given model $\mathcal{M}$, whereas the prior represents the knowledge of the model used for the representation of a phenomenon. With these notations,

$$\mathcal{P}(\mathcal{M}|\boldsymbol{\Theta}) \propto \mathcal{L}(\boldsymbol{\Theta}|\mathcal{M})\mathcal{P}(\mathcal{M}). \tag{4}$$

In this work, the model parameters are $\mathcal{M} = \{\mu = 5\log(r) - 5, A\}$, with μ the distance modulus of the star, r the distance to the star, and A its age. The observables $\boldsymbol{\Theta}$ can be split into the Gaia photometric observables $\boldsymbol{\Theta}_{\rm phot} = \{G_0, BP_0, RP_0, \delta_G, \delta_{BP}, \delta_{RP}\}$ and the Gaia astrometric (parallax) observables $\boldsymbol{\Theta}_{\rm astrom} = \{\varpi, \delta_\varpi\}$, with δx the uncertainty associated with measurement x. Assuming that the photometric and astrometric information on the star are independent, equation (4) becomes

$$\mathcal{P}(\mathcal{M}|\boldsymbol{\Theta}) \propto \mathcal{L}_{\rm phot}(\boldsymbol{\Theta}_{\rm phot}|\mathcal{M})\mathcal{L}_{\rm astrom}(\boldsymbol{\Theta}_\varpi|\mathcal{M})\mathcal{P}(\mathcal{M}). \tag{5}$$

[2] https://gea.esac.esa.int/archive/

Table 1. Physical parameters of the analysed UMPs found in literature. [Fe/H], [C/Fe], v_r, $T_{\rm lit}$, $\log(g)_{\rm lit}$ are from the articles listed in the column References. v_r and the binarity flag denoted with *a* are from Arentsen et al. (2018), the v_r values for binary systems denoted with *a* are the systemic radial velocities corrected for the binary orbital motion. v_r values for stars that are not known to be in a binary system and from the compilation of Arentsen et al. (2018) are calculated with a weighted average of all the v_r measurements. $E(B-V)$ is from Schlegel et al. (1998). In case the star is in a binary system, the binarity flag is equal to Y, while stars labelled with N are not in a binary system or the binarity is not known.

Identifier	α_{J2000} (deg)	δ_{J2000} (deg)	[Fe/H] (dex)	$\delta_{[Fe/H]}$ (dex)	[C/Fe] (dex)	$\delta_{[C/Fe]}$ (dex)	v_r (km s^{-1})	δ_{v_r} (km s^{-1})	$T_{\rm lit}$ (K)	$\delta_{T_{\rm lit}}$ (K)	$\log(g)_{\rm lit}$ (dex)	$\delta_{\log(g)_{\rm lit}}$ (dex)	E(B-V) (mag)	Binarity	References
HE 0020−1741	5.6869167	−17.4080944	−4.05	–	1.4	–	93.06	0.83	4630.0	150	0.95	0.3	0.021	N	Placco et al. (2016)
SDSS J0023+0307	5.80834363858	3.13284420892	<−6.6	–	<2.0	–	−195.5	1.0	6140	132	4.8	0.6	0.028	N	Aguado et al. (2018b)
HE 0044−3755	11.6508144643	−37.6593210379	−4.19	–	−0.3	–	48.3	2.5	4800	100	1.5	0.1	0.010	N	Cayrel et al. (2004)
HE 0057−5959	14.9749409617	−59.7249294278	−4.08	–	0.86	–	375.64a	1.00	5257	–	2.65	–	0.016	N	Norris et al. (2007), Norris et al. (2013)
HE 0107−5240	17.3714810637	−52.4095009821	−5.5	0.2	3.85	–	46.0a	2.0	5100	150	2.2	0.3	0.011	Ya	Christlieb et al. (2004)
HE 0134−1519	24.2724039774	−15.0729979538	−4.0	0.2	1.00	0.26	244	1	5500	100	3.2	0.3	0.016	N	Hansen et al. (2015)
SDSS J014036.21+234458.1	25.1509195676	23.7495011637	−4.0	0.3	1.1	0.3	−197a	1	5703	100	4.7	0.3	0.114	Ya	Yong et al. (2013)
BD+44 493	36.7072451683	44.9629239592	−4.3	0.2	1.2	0.2	−150.14	0.63	5430	150	3.4	0.3	0.079	N	Ito et al. (2013)
HE 0233−0343	39.1241380137	−3.50167460698	−4.7	0.2	3.48	0.24	64	1	6300	100	3.4	0.3	0.022	N	Hansen et al. (2015)
BPS CS 22963−0004	44.1940476203	−4.85483952327	−4.09	0.15	0.40	0.23	292.4	0.2	5060	42	2.15	0.16	0.045	N	Roederer et al. (2014)
SDSS J030444.98+391021.1	46.1874375223	39.1725764233	−4.0	0.2	0.7	–	87	8	5859	13	5.0	0.5	0.111	N	Aguado et al. (2017b)
SMSS J031300.36−670839.3	48.2515614545	−67.1442601577	<−6.53	–	4.5	0.2	298.5a	0.5	5125	–	2.3	–	0.032	N	Keller et al. (2014), Nordlander et al. (2017)
HE 0330+0148	53.158696449	1.96666957231	−4.0	0.1	2.6	–	−33.6a	1.0	4100	200	5.2	0.1	0.094	Y	Plez, Cohen & Meléndez (2005)
HE 0557−4840	89.6636087844	−48.6658029727	−4.8	0.2	1.65	–	211.9	0.8	4900	100	2.2	0.3	0.037	N	Norris et al. (2007)
SDSS J081554.26+472947.5	123.976115075	47.4965559814	<−5.8	–	>5.0	–	−95	23	6215	82	4.7	0.5	0.063	N	Aguado et al. (2018a)
SDSS J092912.32+023817.0	142.301366238	2.63806158906	−4.97	–	<3.91	–	388.3	10.4	5894	–	3.7	–	0.053	Y	Bonifacio et al. (2015), Caffau et al. (2016)
SDSS J094708.27+461010.0	146.784471294	46.1694746754	−4.1	0.2	1.0	0.4	−5	12	5858	73	5.0	0.5	0.013	N	Aguado et al. (2017a)
HE 1012−1540	153.722814524	−15.9314366402	−4.17	0.16	2.2	–	225.8a	0.5	5230	32	2.65	0.2	0.061	N	Roederer et al. (2014)
SDSS J102915+172927	157.313121378	17.4910907404	−4.99	0.06	<0.7	–	−35	4	5850	100	4.0	0.2	0.023	N	Caffau et al. (2011)
SDSS J103402.70+070116.6	158.511301205	7.02129528322	−4.01	0.14	–	–	153	3	6270	–	4.0	–	0.02	N	Bonifacio et al. (2018)
SDSS J103556.11+064143.9	158.983818359	6.6955582264	<−5	–	3.08	–	−45	6	6262	–	4	–	0.024	N	Bonifacio et al. (2015)
SDSS J105519.28+232234.0	163.830333515	23.3761158455	−4.00	0.07	<0.7	–	62	4	6232	28	4.9	0.1	0.015	N	Aguado et al. (2017b)
SDSS J120441.38+120111.5	181.172452065	12.019865284	−4.34	0.05	<1.45	–	51	3	5917	–	3	–	0.024	N	Placco et al. (2015)
SDSS J124719.46−034152.4	191.831114232	−3.69791795379	−4.11	0.18	<1.61	–	84	6	6332	–	4	–	0.022	N	Caffau et al. (2013b)
LAMOST J125346.09+075343.1	193.44189217	7.89526036289	−4.02	0.06	1.59	–	78.0	0.4	6030	135	3.65	0.16	0.025	N	Li et al. (2015)
SDSS J131326.89−001941.4	198.3620349838832	−0.3281488686298	−4.7	0.2	2.8	0.3	268	4	5525	106	3.6	0.5	0.024	Y	Allende Prieto et al. (2015), Frebel et al. (2015), Aguado et al. (2017b)
HE 1310−0536	198.379940261	−5.87014820763	−4.2	0.2	2.36	0.23	113.2	1.7	5000	100	1.9	0.3	0.037	N	Hansen et al. (2015)
HE 1327−2326	202.524748159	−23.6971386187	−5.96	–	3.78	–	64.4a	1.3	6200	100	3.7	0.3	0.066	N	Frebel et al. (2008)
HE 1424−0241	216.668044499	−2.90763517546	−4.05	–	<0.63	–	59.8	0.6	5260	–	2.66	–	0.055	N	Norris et al. (2013), Cohen et al. (2008)
SDSS J144256.37−001542.7	220.734907425	−0.26188939275	−4.09	0.21	<1.59	–	225	9	5850	–	4	–	0.036	N	Caffau et al. (2013a)
Pristine221.8781+9.7844	221.878064787	9.78436859397	−4.66	0.13	<1.76	–	−149.0	0.5	5792	100	3.5	0.5	0.020	N	Starkenburg et al. (2018)
SDSS J164234.48+443004.9	250.643694345	44.5013644484	−4.0	0.2	0.55	0.0	−136	4	6280	150	5.0	0.3	0.011	N	Aguado et al. (2016)
SDSS J173403.91+644633.0	263.516273652	64.7758235012	−4.3	0.2	3.1	0.2	−258	13	6183	78	5.0	0.5	0.028	N	Aguado et al. (2017a)
SDSS J174259.67+253135.8	265.748669215	25.526636261	−4.8	0.07	3.6	0.2	−221.93	10.00	6345	–	4	–	0.055	N	Bonifacio et al. (2015)
2MASS J18082002−5104378	272.083464041	−51.0771900644	−4.07	0.07	<0.5	–	16.54	0.12	5440	100	3.0	0.2	0.101	Y	Meléndez et al. (2016) Schlaufman et al. (2018)
BPS CS 22891−0200	293.829490257	−61.7067706698	−4.06	0.15	–	–	131	10	4490	33	0.5	0.1	0.068	N	Roederer et al. (2014)
BPS CS 22885−0096	305.213220651	−39.8917320574	−4.21	0.07	–	–	−248	10	4580	34	0.75	0.15	0.048	N	Roederer et al. (2014)
BPS CS 22950−0046	305.368323431	−13.2760006492	−4.12	0.14	–	–	111	10	4380	32	0.5	0.1	0.054	N	Roederer et al. (2014)
BPS CS 30336−0049	311.348055352	−28.7099758468	−4.04	0.09	−0.28	0.31	−236.6	0.8	4827	100	1.5	0.2	0.054	N	Lai et al. (2008)
HE 2139−5432	325.676864649	−54.3119357441	−4.02	–	–	–	105a	3	5457	44	2.0	0.2	0.017	Ya	Norris et al. (2013)
HE 2239−5019	340.611864594	−50.0669213083	−4.2	0.2	<1.7	–	368.7	0.5	6100	100	3.5	0.3	0.010	N	Hansen et al. (2015)
HE 2323−0256	351.62419731	−2.66612144628	−4.38	0.15	–	–	−125.8a	0.3	4630	34	0.95	0.13	0.043	N	Roederer et al. (2014)

3.1.1 $\mathcal{L}_{\rm phot}(\boldsymbol{\Theta}_{\rm phot}|\mathcal{M})$

In order to determine the photometric likelihood of a given star for a chosen μ and A, we rely on the isochrone models from the MESA/MIST library (Paxton et al. 2011; Choi et al. 2016; Dotter 2016), as they are the only set of publicly available isochrones that reach the lowest metallicity ([Fe/H] $= -4.0$ dex) and is therefore the most appropriate for our study.

Any isochrone, $\mathcal{I}$, of a given age, A, associated with a luminosity function[3] $\Phi(M_G|A)$, predicts the density distribution triplet of absolute magnitudes $p(M_G, M_{BP}, M_{RP}|\mathcal{I}, \Phi)$ in

[3]This associated luminosity function, Φ, assumes a Salpeter IMF (Salpeter 1955). The choice of the IMF is not very sensitive for the type of stars we analyse.

Table 2. Gaia properties of the stars. Coordinates at J2015.5, the dereddened G_0, BP_0, and RP_0 magnitudes, proper motion μ_α, μ_δ, and the parallax ϖ for the analysed sample of UMPs (https://gea.esac.esa.int/archive/ Gaia Collaboration 2016, 2018) are listed. G_0, BP_0, and RP_0 magnitudes are dereddened using the Schlegel et al. (1998) extinction map. The parallaxes ϖ are not corrected for the offset $\varpi_0 = -0.029$ mas.

Identifier	$\alpha_{J2015.5}$ (deg)	$\delta_{J2015.5}$ (deg)	Gaia id	G_0 (mag)	δ_G (mag)	BP_0 (mag)	δ_{BP} (mag)	RP_0 (mag)	δ_{RP} (mag)	μ_α (mas yr^{-1})	δ_{μ_α} (mas yr^{-1})	μ_δ (mas yr^{-1})	δ_{μ_δ} (mas yr^{-1})	ϖ (mas)	δ_ϖ (mas)
HE 0020−1741	5.68699047782	−17.40811466246	2367173119271988480	12.5609	0.00017	13.0699	0.0010	11.9040	0.0006	14.424	0.064	−4.546	0.043	0.1456	0.0384
SDSS J0023+0307	5.80835977813	3.132743082	2548541852945056896	17.5638	0.001	17.7947	0.0074	17.1246	0.0074	3.743	0.318	−13.912	0.187	0.2697	0.1406
HE 0044−3755	11.65089731416	−37.65935345272	5000753194373767424	11.6633	0.0003	12.1427	0.0009	11.0310	0.0009	15.234	0.061	−7.529	0.041	0.2152	0.0344
HE 0057−5959	14.97496136508	− 59.72497472878	4903905598859396480	15.0507	0.0004	15.3857	0.0025	14.5292	0.0025	2.389	0.042	−10.522	0.041	0.1982	0.0254
HE 0107−5240	17.37149810186	−52.40951706252	4927204800008334464	14.9334	0.0003	15.3232	0.0019	14.3638	0.0019	2.414	0.033	−3.735	0.035	0.0789	0.0258
HE 0134−1519	24.27251527664	−15.07304490506	2453397508316944128	14.2270	0.0003	14.5501	0.0022	13.7181	0.0022	24.961	0.056	−10.905	0.039	0.3454	0.0299
SDSS J014036.21+234458.1	25.15092436121	23.74940873996	290930261314166528	15.0495	0.0006	15.3423	0.0034	14.5750	0.0034	1.019	0.176	−21.466	0.091	1.0482	0.0562
BD+44 493	36.70796538815	44.96278519908	341511064663637376	8.6424	0.0005	8.9634	0.0016	8.1758	0.0016	118.359	0.141	−32.229	0.105	4.7595	0.0660
HE 0233−0343	39.12435352835	−3.50172027632	2495327693479473408	15.2126	0.0005	15.4433	0.0027	14.8029	0.0027	49.962	0.073	−10.607	0.072	0.7925	0.0545
BPS CS 22963−0004	44.1941414394	−4.85485100336	5184426749232471808	14.6906	0.0005	14.9991	0.0024	14.1973	0.0024	21.712	0.058	−2.666	0.059	0.2220	0.0364
SDSS J030444.98+391021.1	46.18743595787	39.17249343121	142874251765330944	17.0085	0.0019	17.3215	0.0088	16.5085	0.0088	−0.282	0.336	−19.276	0.241	0.0752	0.1929
SMSS J031300.36−670839.3	48.25163934361	−67.14425547143	4671418400651900544	14.4342	0.0003	14.8379	0.0018	13.8545	0.0018	7.027	0.032	1.088	0.03	0.0981	0.0162
HE 0330+0148	53.15953261866	1.96344241611	3265069670684495744	13.0859	0.0004	13.8664	0.0032	12.2728	0.0032	194.093	0.453	−749.533	0.499	12.7174	0.2106
HE 0557−4840	89.66361346726	−48.66579980934	4794791782906532608	15.0976	0.0004	15.5156	0.0028	14.4984	0.0028	0.718	0.043	0.735	0.044	0.0389	0.0207
SDSS J081554.26+472947.5	123.97602487635	47.49645166114	931227322991970560	16.5417	0.0006	16.8056	0.0057	16.1052	0.0057	−14.154	0.135	−24.229	0.09	0.4441	0.0837
SDSS J092912.32+023817.0	142.30134736257	2.63804791153	3844818546870217728	17.8302	0.0023	18.1360	0.0316	17.3618	0.0316	−4.379	0.342	−3.177	0.364	0.1276	0.1872
SDSS J094708.27+461010.0	146.78455769932	46.16940656739	821637654725909760	18.7343	0.0021	19.0195	0.0221	18.2783	0.0221	13.898	0.317	−15.819	0.332	0.1989	0.2299
HE 1012−1540	153.7223563828	−15.93131552666	3751852536639575808	13.7019	0.0004	14.0084	0.0033	13.2135	0.0033	−102.32	0.046	28.13	0.04	2.5417	0.0280
SDSS J102915+172927	157.31307233934	17.49107327845	3890626773968983296	16.4857	0.0013	16.7665	0.0062	15.9976	0.0062	−10.863	0.146	−4.056	0.113	0.7337	0.0780
SDSS J103402.70+070116.6	158.51126738928	7.02126631404	3862721340654330112	17.1906	0.0018	17.4051	0.0227	16.7943	0.0063	−7.795	0.236	−6.728	0.291	0.2874	0.1367
SDSS J103556.11+064143.9	158.98383317025	6.69554785085	3862507691800855040	18.3472	0.0034	18.6230	0.0197	17.9584	0.0197	3.416	0.403	−2.41	0.369	−0.3912	0.3163
SDSS J105519.28+232234.0	163.83036912138	23.37606935407	3989873022818570240	17.5182	0.0025	17.7015	0.0317	17.1298	0.0317	7.591	0.291	−10.798	0.324	0.5909	0.1821
SDSS J120441.38+120111.5	181.17245380263	12.01984412118	3919025342543602176	16.0270	0.0005	16.3239	0.0043	15.5497	0.0043	0.395	0.11	−4.915	0.067	0.2454	0.0656
SDSS J124719.46−034152.4	191.83107728926	−3.69791015204	3681866216349964288	18.1908	0.0016	18.3958	0.0118	17.7716	0.0118	−8.562	0.439	1.812	0.226	0.3075	0.2098
LAMOST J125346.09+075343.1	193.44198364753	7.895007511	3733768078624022016	12.2280	0.0002	12.4603	0.0011	11.8239	0.0011	21.045	0.082	−58.727	0.049	1.4053	0.0378
SDSS J131326.89−001941.4	198.36201866349555	−0.32817714440715445	3687441358777986688	16.3560	0.0010	16.7237	0.0058	15.8183	0.0710	−3.790	0.160	−6.567	0.078	0.2976	0.0972
HE 1310−0536	198.37991838382	−5.8701554707	3635533208672382592	14.0256	0.0004	14.5363	0.0021	13.3649	0.0021	−5.054	0.053	−1.687	0.042	0.0078	0.0342
HE 1327−2326	202.52450119109	−23.69694272263	6194815228636688768	13.2115	0.0004	13.4500	0.0019	12.8012	0.0019	−52.524	0.04	45.498	0.035	0.8879	0.0235
HE 1424−0241	216.66802803117	−2.90764744641	3643332182086977792	15.0437	0.0007	15.3934	0.0046	14.5017	0.0046	−3.82	0.087	−2.85	0.066	0.1152	0.0469
SDSS J144256.37−001542.7	220.73490626598	−0.26186035888	3651420563283262208	17.5635	0.0023	17.8216	0.0277	17.1364	0.0277	−0.269	0.315	6.743	0.396	−0.3910	0.2981
Pristine221.8781+9.7844	221.87803086877	9.78436834556	1174522686140620672	16.1846	0.0009	16.4688	0.0053	15.7060	0.0053	−7.763	0.110	−0.058	0.116	0.1187	0.0940
SDSS J164234.48+443004.9	250.643641407	44.50138608236	1405755062407483520	17.4658	0.0012	17.6987	0.0112	17.0356	0.0112	−8.769	0.149	5.025	0.244	0.3122	0.0906
SDSS J173403.91+644633.0	263.51630029934	64.77581642801	1632736765377141632	19.1198	0.0038	19.3849	0.0465	18.7074	0.0465	2.638	0.44	−1.643	0.553	−0.1052	0.2702
SDSS J174259.67+253135.8	265.74864014534	25.52658646063	4581822389265279232	18.5115	0.0022	18.7628	0.0248	18.0991	0.0248	−6.093	0.248	−11.567	0.292	−0.1628	0.1870
2MASS J18082002−5104378	272.08342547713	−51.07724449784	6702907209758894848	11.4880	0.0003	11.7853	0.0024	11.0119	0.0024	−5.627	0.068	−12.643	0.058	1.6775	0.0397
BPS CS 22891−0200	293.82944462026	−61.70676742367	6445220927325014016	13.4478	0.0003	13.9306	0.0017	12.8053	0.0017	−5.024	0.053	0.754	0.036	0.1135	0.0342
BPS CS 22885−0096	305.21319576813	−39.89176180812	6692925538259931136	12.9385	0.0003	13.3482	0.0017	12.3514	0.0017	−4.434	0.038	−6.91	0.028	0.1708	0.0247
BPS CS 22950−0046	305.36833037469	−13.27600846442	6876806419780834048	13.7403	0.0002	14.2631	0.0011	13.0627	0.0011	1.57	0.045	−1.815	0.028	0.0587	0.0270
BPS CS 30336−0049	311.34804708033	−28.71001086007	6795730493933072128	13.5803	0.0002	14.0740	0.0013	12.9283	0.0013	−1.685	0.038	−8.132	0.027	0.0418	0.0227
HE 2139−5432	325.676883449	−54.31195504869	6461736966363075200	14.9386	0.0003	15.2991	0.0017	14.4000	0.0017	2.547	0.046	−4.484	0.041	−0.0067	0.0298
HE 2239−5019	340.61191653735	−50.06702317874	6513870718215626112	15.6038	0.0007	15.8336	0.0034	15.2107	0.0034	7.744	0.054	−23.66	0.076	0.2200	0.0545
HE 2323−0256	351.6242048175	−2.66612932812	2634585342263017984	13.9922	0.0004	14.4286	0.0031	13.3832	0.0031	1.742	0.062	−1.831	0.048	0.0038	0.0359

the Gaia photometric bands. After computing the likelihood $p(\mathbf{\Theta}_{\rm phot}|M_G, M_{BP}, M_{RP}, \mu)$, of these predictions shifted to a distance modulus μ, against the observed photometric properties of the star, $\mathcal{L}_{\rm phot}$ results from the marginalization along that isochrone:

$$\begin{aligned}\mathcal{L}_{\rm phot}(\mathbf{\Theta}_{\rm phot}|\mu, A, \Phi) &= \int_{\mathcal{I}} p(\mathbf{\Theta}_{\rm phot}|M_G, M_{BP}, M_{RP}, \mu) \\ &\quad \times p(M_G, M_{BP}, M_{RP}|\mathcal{I}, \Phi) p(\mathcal{I}|A) d\mathcal{I}, \end{aligned} \quad (6)$$

with

$$\begin{aligned} p(\mathbf{\Theta}_{\rm phot}|M_G, M_{BP}, M_{RP}, \mu) &= \mathcal{N}(G_0|M_G + \mu, \delta_G^2 + 0.01^2) \\ &\quad \times \mathcal{N}((BP - RP)_0|M_{BP} - M_{RP}, \delta_{BP}^2 + \delta_{RP}^2 + 2 \times 0.01^2) \end{aligned} \quad (7)$$

and $\mathcal{N}(x|m, s^2)$ the value of a Gaussian function of mean m and variance s^2 taken on x. In equation (7), a systematic uncertainty of 0.01 mag is added to the photometric uncertainties in each band to represent the uncertainties on the models.

For most stars, we expect to find two peaks in $\mathcal{L}_{\rm phot}(\mathbf{\Theta}_{\rm phot}|\mathcal{M})$, corresponding to the dwarf and giant solutions but stars close to the main sequence turnoff naturally yield a PDF with a single peak.

3.1.2 $\mathcal{L}_{\rm astrom}(\mathbf{\Theta}_\varpi|\mathcal{M})$

Gaia DR2 provides us with a parallax ϖ and its uncertainty δ_ϖ, which is instrumental in breaking the dwarf/giant distance degeneracy for most stars. The astrometric likelihood is trivially

defined as

$$\mathcal{L}_{\rm astrom}(\varpi\,|\delta_\varpi, r) = \frac{1}{\sqrt{2\pi}\delta_\varpi}\exp\left(-\frac{1}{2}\left(\frac{\varpi-\varpi_0-r^{-1}}{\delta_\varpi}\right)^2\right). \quad (8)$$

Here, $\varpi_0 = -0.029$ mas is the parallax zero-point offset measured by Lindegren et al. (2018).

Even in cases for which the parallax is small and the associated uncertainties are large, the Gaia data are often informative enough to rule out a nearby (dwarf) solution.

3.1.3 $\mathcal{P}(\mathcal{M})$

Prior on the distance and position $(r|\ell, b)$ — The prior on the distance and position to the star folds in our knowledge of the distribution of UMP stars around the MW. Since we expect those stars to be among the oldest stars of the MW and (likely) accreted, we first assume a halo profile. In particular, we use the RR Lyrae density power-law profile inferred by Hernitschek et al. (2018), $\rho(r) \propto r^{-3.4}$, since RR Lyrae stars are also expected to be old halo tracers.

From this stellar density profile, the probability density to have a star at distance r from the Sun along the line of sight described by Galactic coordinates (ℓ, b) is

$$\mathcal{P}_{\rm H}(r|\ell, b) = \rho_0 r^2\left(\frac{D_{\rm GC}(r|\ell, b)}{r_0}\right)^{-3.4}. \quad (9)$$

In this equation, $D_{\rm GC}(r|\ell, b)$ is the distance of the star to the Galactic centre, while ρ_0 and r_0 are reference values for the density and the scalelength of the halo. For this work, the specific values of ρ_0 and r_0 will not affect the result because they will be simplified during the normalization of the posterior PDF.

Anticipating the results described in Section 4, we find that, even when using a pure halo prior, ∼26 per cent of our sample remains confined to the MW plane and the distance inference for a small number of stars yields unrealistic (unbound) orbits. Hence we repeat the analysis described with a mixture of a thick disc and a halo prior to investigate if, and how, the choice of the prior affects our results. This alternative MW prior is defined as

$$\mathcal{P}_{\rm DH}(r|\ell, b) = \eta\mathcal{P}_{\rm D,norm}(r|\ell, b) + (1-\eta)\mathcal{P}_{\rm H,norm}(r|\ell, b), \quad (10)$$

with $\eta = 1/2$ the mixture coefficient, $\mathcal{P}_{\rm H,norm}(r|\ell, b)$ the normalized halo prior expressed in equation (9), and $\mathcal{P}_{\rm D,norm}(r|\ell, b)$ the normalized thick disc prior defined by Binney & Tremaine (2008):

$$\mathcal{P}_{\rm D}(r|\ell, b) = \frac{r^2\Sigma_{\rm T}}{2z_{\rm T}}\exp\left(-\frac{D_{\rm GC}(r, \ell, b)}{D_{\rm T}} - \frac{|z|}{z_{\rm T}}\right), \quad (11)$$

with $\Sigma_{\rm T} = 268.648\,{\rm M}_\odot\,{\rm pc}^{-2}$ the disc surface density, $D_{\rm T} = 2$ kpc the radial scalelength for the density and $z_{\rm T} = 0.9$ kpc the vertical scalelength (Bland-Hawthorn & Gerhard 2016).

Prior on the age A, $\mathcal{P}(A)$ — There is no well defined age constraint for UMP stars, but they are usually assumed to be very old (Starkenburg et al. 2017b). Hence we assume that all the stars studied here were formed at least 11.2 Gyr ago ($\log(A/{\rm yr}) = 10.05$). Beyond this age, we assume a uniform prior on $\log(A)$ until 14.1 Gyr ($\log(A/{\rm yr}) = 10.15$), which is the maximum value of the isochrone grid.

Finally, $\mathcal{P}(\mathcal{M}) = \mathcal{P}(r|\ell, b)\mathcal{P}(A)$.

3.1.4 *Posterior PDF on distance* r

So far, $\mathcal{M} = \{\mu, A\}$ but we aim to infer the PDF on the distance modulus (or the distance) to the star alone. In order to do so, we simply marginalize over the age:

$$P(r = 10^{(\mu+5)/5}|\boldsymbol{\Theta}) = \int \mathcal{P}(\mathcal{M}|\boldsymbol{\Theta})dA, \quad (12)$$

assuming $\mu \geq 0$ mag ($r \geq 10$ pc).

3.2 Effective temperature and surface gravity inference

For each point of the theoretical isochrones $\mathcal{I}(A, \mu)$ corresponds a value of the surface gravity, $\log(g)$, and a value of the effective temperature, $T_{\rm eff}$. Marginalizing the likelihood and prior over distance modulus and age instead of over the isochrone as in equation (6), we can find the posterior probability as a function of $\log(g)$ and $T_{\rm eff}$. In detail,

$$\mathcal{P}(\log(g), T_{\rm eff}|\boldsymbol{\Theta}) = \iint \mathrm{P}(\boldsymbol{\Theta}|\log(g), T_{\rm eff}, \mathcal{I}(A), \mu) \times \Phi(M(\log(g), T_{\rm eff}, A))\mathcal{P}(r, \ell, b)\mathcal{L}_{\rm astrom}(\varpi\,|r(\mu), \delta_\varpi)\,{\rm dA}\,{\rm d}\mu. \quad (13)$$

3.3 Orbital inference

Gaia DR2 provides proper motions in right ascension and declination with their associated uncertainties and covariance. Combining this with the distance inferred through our analysis, we can calculate the velocity vector PDF $P(\boldsymbol{v}) = P(v_r, v_\alpha, v_\delta)$ for all 42 stars in our UMPs sample. This PDF, in turn, allows us to determine the properties of the orbit of the stars for a given choice of Galactic potential. We rely on the `galpy`[4] package (Bovy 2015) and choose their *MWPotential14*, which is a MW gravitational potential composed of a power law, exponentially cut-off bulge, a Miyamoto Nagai Potential disc, and a Navarro, Frenk & White (1997) dark matter halo. A more massive halo is chosen for this analysis, with a mass of $1.2 \cdot 10^{12}\,{\rm M}_\odot$ compatible with the value from Bland-Hawthorn & Gerhard (2016; versus $0.8 \cdot 10^{12}\,{\rm M}_\odot$ for the halo used in *MWPotential14*).

For each star, we perform a thousand random drawings from the position, distance, radial velocity, and proper motion PDFs. In the case of the two components of the proper motion (μ_α, μ_δ), we consider their correlation given by the coefficients in *Gaia DR2*, drawing randomly these two parameters according to a multivariate Gaussian function that takes into account the correlation. The possible correlation between coordinates and proper motions is not taken into account because it does not affect our result. For each drawing, we integrate this starting phase-space position backwards and forwards for 2 Gyr and extract the apocentre, $r_{\rm apo}$, pericentre, $r_{\rm peri}$, eccentricity, ε, energy E, the angular momentum L of the resulting orbit (note that in this frame of reference, $L_z > 0$ means a prograde orbit), and the action-angle vector ($J_r, J_\phi = L_z, J_z$, where the units are in km s^{-1} kpc).

4 RESULTS

Tables 3 and 4 summarize the results of the analysis and list the inferred stellar and orbital properties for all stars, respectively. In cases for which the (distance) PDF is double-peaked, we report the two solutions along with their fractional probability.

Fig. 1 shows the colour-magnitude diagram (CMD) and the temperature-surface gravity diagram for our UMP sample, plot-

[4] http://github.com/jobovy/galpy

Table 3. Inferred stellar parameters for the stars in the sample. Distances D, effective temperatures T_{eff} and surface gravities log(g) obtained in this work for the UMPs sample. If a second peak in the PDF is present, an estimate of the subtended area around the two peaks within $\pm 3\sigma$ is shown (Area= $\int_{d_1-3\sigma}^{d_1+3\sigma} P(r)\mathrm{d}r$). The column *Prior* indicates the MW prior used for inferring the parameters (i.e. H means halo prior, D+H indicates the disc+halo prior).

Identifier	D (kpc)	δ_D (kpc)	T_{eff} (K)	$\delta_{T_{eff}}$ (K)	log(g) (dex)	$\delta_{log(g)}$ (dex)	Area	Prior
HE 0020−1741	10.3	0.4	4774	20	1.05	0.05		H
	10.3	0.4	4774	20	1.05	0.05		D+H
SDSS J0023+0307	2.710	0.139	6116	66	4.6	0.1	88%	H
	11.03	0.73	6047	146	3.4	0.1	12%	H
	2.693	0.136	6108	65	4.6	0.1	99.6%	D+H
	11.02	0.74	6050	154	3.4	0.1	0.4%	D+H
HE 0044−3755	5.70	0.25	4852	22	1.2	0.1		H
	5.65	0.26	4863	23	1.2	0.1		D+H
HE 0057−5959	6.80	0.71	5483	42	2.7	0.1		H
	6.50	0.72	5501	44	2.7	0.1		D+H
HE 0107−5240	14.3	1.0	5141	32	1.9	0.1		H
	14.2	1.0	5141	32	1.9	0.1		D+H
HE 0134−1519	3.75	0.33	5572	90	2.9	0.1		H
	3.61	0.30	5589	37	2.9	0.1		D+H
SDSS J014036.21+234458.1	0.762	0.022	5963	41	4.6	0.1		H
	0.761	0.022	5962	40	4.6	0.1		D+H
BD+44 493	0.211	0.003	5789	19	3.2	0.1		H
	0.211	0.003	5794	20	3.2	0.1		D+H
HE 0233−0343	1.090	0.043	6331	47	4.5	0.1		H
	1.088	0.043	6327	47	4.5	0.1		D+H
BPS CS 22963−0004	4.47	0.42	5589	42	2.9	0.1		H
	4.36	0.39	5601	43	3.0	0.1		D+H
SDSS J030444.98+391021.1	14.9	1.3	5547	39	2.8	0.1	99%	H
	1.505	0.071	5649	68	4.7	0.1	1%	H
	14.3	2.5	5548	74	2.8	0.2	79%	D+H
	1.503	0.071	5648	68	4.7	0.1	21%	D+H
SMSS J031300.36−670839.3	12.0	0.8	5111	31	1.8	0.1		H
	12.1	0.8	5111	32	1.8	0.1		D+H
HE 0330+0148	0.075	0.001	4454	1	5.0	0.1		H
	0.075	0.001	4460	1	5.0	0.1		D+H
HE 0557−4840	20.0	1.3	5017	28	1.6	0.1		H
	20.0	1.3	5018	30	1.6	0.1		D+H
SDSS J081554.26+472947.5	1.591	0.067	6034	56	4.6	0.1		H
	1.588	0.066	6031	56	4.6	0.1		D+H
SDSS J092912.32+023817.0	15.6	2.6	5708	124	3.1	0.2	68%	H
	2.398	0.205	5775	122	4.7	0.1	32%	H
	2.367	0.198	5756	120	4.7	0.1	95%	D+H
	15.5	2.6	5713	125	3.1	0.2	5%	D+H
SDSS J094708.27+461010.0	3.84	0.30	5854	110	4.7	0.1	82%	H
	21.9	2.0	5801	118	3.2	0.1	18%	H
	3.76	0.28	5823	55	4.7	0.1	98%	D+H
	21.9	2.0	5802	120	3.2	0.1	2%	D+H
HE 1012−1540	0.384	0.004	5872	16	4.7	0.1		H
	0.384	0.004	5870	16	4.7	0.1		D+H
SDSS J102915+172927	1.281	0.051	5764	57	4.7	0.1		H
	1.278	0.050	5761	56	4.7	0.1		D+H
SDSS J103402.70+070116.6	2.79	0.26	6366	110	4.5	0.1	89%	H
	8.28	0.64	6333	211	3.6	0.1	11%	H
	2.75	0.25	6330	110	4.5	0.1	99.4%	D+H
	8.18	0.65	6320	200	3.6	0.1	0.6%	D+H
SDSS J103556.11+064143.9	3.97	0.35	6144	110	4.6	0.1	67%	H
	15.6	1.2	6072	168	3.5	0.1	33%	H
	3.88	0.32	6114	106	4.6	0.1	95.5%	D+H
	15.6	1.2	6073	175	3.5	0.1	0.5%	D+H
SDSS J105519.28+232234.0	3.49	0.45	6452	147	4.5	0.1	96%	H
	8.84	0.94	6581	248	3.8	0.2	4%	H
	3.30	0.39	6387	138	4.5	0.1	99.7%	D+H
	8.79	0.99	6606	257	3.8	0.2	0.3%	D+H
SDSS J120441.38+120111.5	7.03	0.54	5679	56	3.1	0.1		H
	6.96	0.53	5686	59	3.1	0.1		D+H

Table 3 – *continued*

Identifier	D (kpc)	δ_D (kpc)	$T_{\rm eff}$ (K)	$\delta_{T_{\rm eff}}$ (K)	log(g) (dex)	$\delta_{\log(g)}$ (dex)	Area	Prior
SDSS J124719.46−034152.4	4.17	0.32	6296	92	4.5	0.1	92%	H
	13.5	1.0	6256	196	3.6	0.1	8%	H
	4.09	0.30	6273	90	4.5	0.1	99%	D+H
	13.4	1.0	6263	205	3.6	0.1	1%	D+H
LAMOST J125346.09+075343.1	0.766	0.016	6598	52	3.8	0.1		H
	0.766	0.016	6608	52	3.8	0.1		D+H
SDSS J131326.89−001941.4	8.59	2.86	5649	171	3.1	0.3	99.96%	H
	1.765	0.248	6278	171	4.5	0.1	0.04%	H
	8.07	2.70	5687	185	3.1	0.3	96.85%	D+H
	1.707	0.227	6237	164	4.6	0.1	3.15%	D+H
HE 1310−0536	20.6	0.9	4788	20	1.0	0.1		H
	20.6	0.9	4764	21	1.0	0.1		D+H
HE 1327−2326	1.212	0.024	6581	52	3.8	0.1		H
	1.212	0.024	6591	51	3.8	0.1		D+H
HE 1424−0241	10.3	1.0	5308	40	2.3	0.1		H
	10.3	1.0	5308	40	2.3	0.1		D+H
SDSS J144256.37−001542.7	11.3	1.0	5993	165	3.4	0.1	87%	H
	2.683	0.266	6104	128	4.6	0.1	13%	H
	2.634	0.249	6079	124	4.6	0.1	84%	D+H
	11.3	1.0	5998	172	3.4	0.1	16%	D+H
Pristine221.8781+9.7844	7.36	0.55	5700	63	3.1	0.1		H
	7.28	0.52	5710	65	3.1	0.1		D+H
SDSS J164234.48+443004.9	2.66	0.16	6149	77	4.6	0.1	99%	H
	10.2	0.7	6126	163	3.5	0.1	1%	H
	2.64	0.16	6140	76	4.6	0.1	99.95%	D+H
	10.1	0.7	6148	172	3.5	0.1	0.05%	D+H
SDSS J173403.91+644633.0	5.46	1.02	6094	233	4.6	0.1	86%	H
	21.8	3.0	6131	297	3.5	0.2	14%	H
	5.05	0.79	5992	208	4.6	0.1	97%	D+H
	21.7	3.0	6134	302	3.5	0.2	3%	D+H
SDSS J174259.67+253135.8	4.46	0.52	6194	145	4.6	0.1	63%	H
	16.6	1.4	6115	198	3.5	0.1	37%	H
	4.34	0.48	6162	140	4.6	0.1	94%	D+H
	16.5	1.4	6118	206	3.5	0.1	6%	D+H
2MASS J18082002−5104378	0.647	0.012	6124	44	3.5	0.1		H
	0.647	0.012	6133	44	3.5	0.1		D+H
BPS CS 22891−0200	14.7	0.5	4789	2	1.2	0.1		H
	13.6	0.6	4836	22	1.2	0.1		D+H
BPS CS 22885−0096	6.65	0.22	5068	16	1.7	0.1		H
	6.61	0.38	5070	27	1.7	0.1		D+H
BPS CS 22950−0046	19.1	0.3	<4780	–	<1.0	–		H
	19.1	0.3	<4780	–	<1.0	–		D+H
BPS CS 30336−0049	15.5	0.7	4809	20	1.1	0.1		H
	15.5	0.7	4802	21	1.1	0.1		D+H
HE 2139−5432	11.0	0.9	5259	34	2.1	0.1		H
	11.0	0.9	5259	34	2.1	0.1		D+H
HE 2239−5019	4.19	0.28	6195	179	3.5	0.1		H
	4.13	0.16	6411	100	3.6	0.1		D+H
HE 2323−0256	14.2	0.6	4937	22	1.4	0.1		H
	14.2	0.6	4937	22	1.4	0.1		D+H

ted with three isochrones that cover the age range we considered ($\log(A/\mathrm{yr}) = 10.05, 10.10, 10.15$). For stars for which the dwarf/giant degeneracy is not broken, we show both solutions connected by a dot–dashed line, where the least probable solution is marked with a dot–dashed ellipse. Only results using a MW halo prior are shown here. As we can see, from the CMD plot (left-hand panel of Fig. 1), the method overall works well, except for the HE 0330+0148 ($(BP - RP)_0 \approx 1.6$ mag) that lays outside the colour range of the available set of isochrones. This special case is discussed in more detail in section A13 (available Online). The distances and stellar parameters lead to the conclusion that 18 stars (∼43 per cent) are in the main sequence phase, and the other 24 are in the subgiant/giant phase (∼57 per cent). This is of course a result of the observing strategies of the multiple surveys that led to the discovery of these stars.

Table 4. Inferred orbital parameters of the stars in the sample. Position (X,Y,Z), the apocentre and pericentre distances in the galactocentric frame, the velocity (U,V,W) in the heliocentric frame, the eccentricity $\varepsilon = (r_{\rm apo} - r_{\rm peri})/(r_{\rm apo} + r_{\rm peri})$ of the orbit, the z-component of the angular momentum, the energy and the kind of orbit (IH = inner halo with $r_{\rm apo} < 30$ kpc, OH = outer halo with $r_{\rm apo} > 30$ kpc, P = close to the MW plane, S = possible Sgr stream member, ω = possible ωCen member) are listed. For the unbound orbits, all the orbital parameters and the kind of orbit are denoted by NB.

Identifier	X (kpc)	Y (kpc)	Z (kpc)	U (km s^{-1})	V (km s^{-1})	W (km s^{-1})	Apo (kpc)	Peri (kpc)	ε	L_z (km s^{-1} kpc)	E (km^2 s^{-2})	Orbit
HE 0020−1741	$7.909^{+0.0}_{-0.0}$	$1.84^{+0.0}_{-0.0}$	$-8.846^{+0.0}_{-0.0}$	$-428.7^{+0.0}_{-0.0}$	$-446.4^{+0.0}_{-0.0}$	$-192.2^{+0.0}_{-0.0}$	$295.8^{+0.0}_{-0.0}$	$12.0^{+0.0}_{-0.0}$	$0.92^{+0.0}_{-0.0}$	$-2311.5^{+0.0}_{-0.0}$	$63046.1^{+0.0}_{-0.0}$	IH
SDSS J0023+0307	$8.456^{+0.039}_{-0.026}$	$1.311^{+0.113}_{-0.075}$	$-2.375^{+0.133}_{-0.199}$	$76.8^{+3.9}_{-5.2}$	$-251.2^{+8.6}_{-12.9}$	$69.2^{+8.1}_{-5.4}$	$9.8^{+0.0}_{-0.0}$	$0.6^{+0.1}_{-0.1}$	$0.88^{+0.03}_{-0.04}$	$108.2^{+97.9}_{-65.3}$	$-68950.0^{+0.0}_{-0.0}$	IH
	NB	NB	NB	NB	NB	NB	NB	NB	NB	NB	NB	NB
HE 0044−3755	$7.353^{+0.028}_{-0.036}$	$-0.824^{+0.036}_{-0.045}$	$-5.61^{+0.246}_{-0.308}$	$-235.9^{+11.0}_{-12.9}$	$-397.1^{+17.8}_{-22.0}$	$-18.1^{+2.5}_{-2.9}$	$21.8^{+4.6}_{-3.0}$	$4.5^{+0.7}_{-0.7}$	$0.66^{+0.01}_{-0.01}$	$-885.7^{+102.1}_{-134.0}$	$-35273.2^{+6822.9}_{-5458.3}$	IH
HE 0057−5959	$6.077^{+0.187}_{-0.22}$	$-3.206^{+0.312}_{-0.367}$	$-5.839^{+0.568}_{-0.668}$	$206.5^{+10.9}_{-9.8}$	$-456.5^{+26.5}_{-29.9}$	$-129.0^{+20.5}_{-19.4}$	$31.3^{+10.2}_{-5.9}$	$9.0^{+0.4}_{-0.3}$	$0.56^{+0.07}_{-0.06}$	$-1947.5^{+229.5}_{-256.5}$	$-20642.9^{+9464.8}_{-6625.3}$	OH
HE 0107−5240	$5.255^{+0.167}_{-0.191}$	$-5.497^{+0.334}_{-0.382}$	$-12.877^{+0.782}_{-0.894}$	$12.5^{+2.4}_{-2.0}$	$-294.3^{+18.3}_{-19.5}$	$77.2^{+8.7}_{-7.7}$	$15.9^{+1.0}_{-0.9}$	$3.2^{+1.5}_{-1.0}$	$0.66^{+0.08}_{-0.1}$	$-354.3^{+98.9}_{-105.5}$	$-46879.6^{+3604.2}_{-3604.2}$	IH
HE 0134−1519	$9.025^{+0.103}_{-0.082}$	$0.244^{+0.025}_{-0.019}$	$-3.679^{+0.291}_{-0.369}$	$-302.5^{+18.8}_{-23.8}$	$-416.8^{+34.1}_{-43.2}$	$-197.1^{+3.7}_{-3.3}$	$70.2^{+49.3}_{-20.7}$	$4.1^{+5.9}_{-0.6}$	$0.87^{+0.02}_{-0.07}$	$-1555.1^{+313.6}_{-425.6}$	$2196.4^{+16677.9}_{-10006.7}$	OH
SDSS J014036.21+234458.1	$8.447^{+0.023}_{-0.025}$	$0.414^{+0.021}_{-0.023}$	$-0.473^{+0.027}_{-0.024}$	$132.8^{+3.6}_{-3.6}$	$-153.5^{+3.6}_{-4.3}$	$61.5^{+4.2}_{-4.7}$	$11.4^{+0.2}_{-0.1}$	$2.5^{+0.1}_{-0.1}$	$0.64^{+0.02}_{-0.02}$	$884.9^{+29.2}_{-30.8}$	$-61399.9^{+465.4}_{-413.7}$	P
BD+44 493	$8.157^{+0.005}_{-0.005}$	$0.131^{+0.004}_{-0.004}$	$-0.054^{+0.002}_{-0.002}$	$30.6^{+2.4}_{-2.6}$	$-184.5^{+2.7}_{-2.8}$	$51.8^{+0.4}_{-0.4}$	$8.3^{+0.0}_{-0.0}$	$1.5^{+0.2}_{-0.1}$	$0.69^{+0.01}_{-0.03}$	$549.6^{+21.8}_{-22.6}$	$-76078.3^{+236.5}_{-236.5}$	P
HE 0233−0343	$8.62^{+0.04}_{-0.04}$	$0.063^{+0.004}_{-0.004}$	$-0.913^{+0.061}_{-0.056}$	$-175.5^{+9.0}_{-8.6}$	$-209.8^{+13.8}_{-13.3}$	$27.5^{+5.0}_{-5.2}$	$11.9^{+0.5}_{-0.4}$	$1.0^{+0.3}_{-0.3}$	$0.85^{+0.04}_{-0.05}$	$344.6^{+119.0}_{-114.2}$	$-62501.0^{+1475.7}_{-1248.6}$	P
BPS CS 22963−0004	$10.739^{+0.268}_{-0.231}$	$-0.087^{+0.007}_{-0.008}$	$-3.62^{+0.304}_{-0.352}$	$-421.8^{+20.9}_{-24.0}$	$-359.1^{+29.5}_{-34.1}$	$-39.2^{+19.1}_{-16.6}$	$155.8^{+183.4}_{-55.0}$	$3.0^{+8.7}_{-1.1}$	$0.96^{+0.0}_{-0.01}$	$-1134.0^{+337.8}_{-391.2}$	$25397.6^{+15195.6}_{-11396.7}$	OH
SDSS J030444.98+391021.1	NB	NB	NB	NB	NB	NB	NB	NB	NB	NB	NB	NB
	$9.24^{+0.063}_{-0.059}$	$0.735^{+0.037}_{-0.035}$	$-0.435^{+0.021}_{-0.022}$	$-77.0^{+6.6}_{-7.0}$	$-33.8^{+5.1}_{-5.8}$	$-139.9^{+6.8}_{-6.1}$	$16.5^{+1.1}_{-1.0}$	$7.9^{+0.1}_{-0.1}$	$0.35^{+0.03}_{-0.03}$	$1960.2^{+38.6}_{-47.4}$	$-40260.6^{+1798.9}_{-1574.0}$	IH
SMSS J031300.36−670839.3	$5.821^{+0.134}_{-0.16}$	$-8.413^{+0.516}_{-0.619}$	$-8.566^{+0.526}_{-0.631}$	$-218.6^{+18.4}_{-19.5}$	$-459.4^{+16.2}_{-18.2}$	$-32.7^{+12.9}_{-12.2}$	$40.4^{+14.7}_{-7.8}$	$5.8^{+1.5}_{-1.5}$	$0.76^{+0.02}_{-0.01}$	$519.6^{+227.0}_{-176.6}$	$-14038.7^{+9814.5}_{-7633.5}$	OH
HE 0330+0148	$8.055^{+0.002}_{-0.002}$	$-0.003^{+0.0}_{-0.0}$	$-0.049^{+0.002}_{-0.002}$	$106.0^{+8.6}_{-9.1}$	$-240.9^{+9.1}_{-11.1}$	$-71.1^{+8.1}_{-8.1}$	$9.0^{+0.6}_{-0.0}$	$0.5^{+0.3}_{-0.2}$	$0.89^{+0.04}_{-0.06}$	$83.2^{+73.0}_{-89.8}$	$-72495.6^{+717.6}_{-717.6}$	P
HE 0557−4840	$12.281^{+0.27}_{-0.254}$	$-17.142^{+1.012}_{-1.075}$	$-9.58^{+0.566}_{-0.601}$	$-110.0^{+5.3}_{-5.9}$	$-203.0^{+2.8}_{-3.1}$	$-32.5^{+6.1}_{-4.4}$	$23.4^{+1.2}_{-1.1}$	$8.2^{+0.9}_{-0.7}$	$0.48^{+0.02}_{-0.03}$	$2273.1^{+186.3}_{-165.6}$	$-29646.0^{+2020.2}_{-2272.7}$	IH
SDSS J081554.26+472947.5	$9.332^{+0.082}_{-0.091}$	$0.185^{+0.011}_{-0.013}$	$0.892^{+0.055}_{-0.061}$	$-12.2^{+18.0}_{-18.0}$	$-176.1^{+12.1}_{-9.9}$	$-156.2^{+12.6}_{-15.2}$	$9.7^{+0.2}_{-0.2}$	$5.0^{+0.5}_{-0.5}$	$0.32^{+0.04}_{-0.03}$	$705.3^{+101.9}_{-92.2}$	$-59940.5^{+2067.3}_{-1447.1}$	IH
SDSS J092912.32+023817.0	$9.225^{+0.165}_{-0.064}$	$-1.502^{+0.203}_{-0.078}$	$1.401^{+0.189}_{-0.073}$	$-218.9^{+9.2}_{-5.2}$	$-275.2^{+13.3}_{-7.8}$	$178.3^{+1.6}_{-2.4}$	$23.5^{+2.6}_{-1.4}$	$2.7^{+0.3}_{-0.1}$	$0.79^{+0.04}_{-0.02}$	$91.4^{+71.5}_{-48.8}$	$-33988.5^{+3752.4}_{-2170.6}$	IH/S
	$16.138^{+0.072}_{-0.234}$	$-9.971^{+0.088}_{-0.287}$	$9.303^{+0.082}_{-6.944}$	$-321.7^{+9.5}_{-43.6}$	$-447.3^{+4.7}_{-35.4}$	$-102.6^{+1.1}_{-40.7}$	$193.7^{+17.6}_{-11.8}$	$21.1^{+0.1}_{-0.4}$	$0.8^{+0.02}_{-0.01}$	$-51.8^{+197.4}_{-928.4}$	$34372.9^{+3808.7}_{-2625.2}$	OH
SDSS J094708.27+461010.0	$10.521^{+0.216}_{-0.189}$	$0.326^{+0.028}_{-0.024}$	$2.941^{+0.251}_{-0.22}$	$205.0^{+18.6}_{-16.3}$	$-264.7^{+20.6}_{-22.1}$	$197.6^{+22.6}_{-18.8}$	$30.0^{+11.4}_{-5.7}$	$8.2^{+0.8}_{-0.8}$	$0.58^{+0.07}_{-0.05}$	$-71.0^{+198.5}_{-213.8}$	$-21786.8^{+9921.8}_{-7717.0}$	OH
	NB	NB	NB	NB	NB	NB	NB	NB	NB	NB	NB	NB
HE 1012−1540	$8.074^{+0.002}_{-0.002}$	$-0.316^{+0.008}_{-0.008}$	$0.207^{+0.005}_{-0.005}$	$-222.5^{+4.3}_{-4.6}$	$-191.1^{+0.4}_{-0.4}$	$49.0^{+1.9}_{-1.8}$	$14.0^{+0.3}_{-0.3}$	$1.3^{+0.1}_{-0.0}$	$0.83^{+0.0}_{-0.01}$	$552.7^{+3.7}_{-3.7}$	$-55562.1^{+850.4}_{-850.4}$	P
SDSS J102915+172927	$8.537^{+0.038}_{-0.033}$	$-0.481^{+0.03}_{-0.034}$	$1.062^{+0.075}_{-0.066}$	$-31.1^{+3.4}_{-3.6}$	$-23.7^{+2.7}_{-3.3}$	$-68.7^{+3.9}_{-4.4}$	$10.9^{+0.3}_{-0.2}$	$8.6^{+0.0}_{-0.0}$	$0.12^{+0.01}_{-0.01}$	$1952.3^{+15.6}_{-19.6}$	$-49546.0^{+552.3}_{-552.3}$	P
SDSS J103402.70+070116.6	$8.917^{+0.075}_{-0.094}$	$-1.482^{+0.122}_{-0.153}$	$2.209^{+0.181}_{-0.227}$	$-97.0^{+1.2}_{-3.4}$	$-178.5^{+6.2}_{-8.9}$	$35.4^{+7.0}_{-11.0}$	$10.2^{+0.1}_{-0.2}$	$2.3^{+0.2}_{-0.3}$	$0.63^{+0.03}_{-0.04}$	$775.0^{+41.4}_{-55.4}$	$-65816.8^{+49.8}_{-102.9}$	P
	$10.714^{+0.263}_{-0.02}$	$-4.385^{+0.425}_{-0.033}$	$6.535^{+0.633}_{-0.241}$	$-188.8^{+36.2}_{-1.5}$	$-366.7^{+24.4}_{-0.1}$	$-126.1^{+38.5}_{-0.8}$	$24.3^{+17.8}_{-0.0}$	$9.3^{+2.1}_{-0.1}$	$0.46^{+0.12}_{-0.0}$	$-426.0^{+81.6}_{-27.7}$	$-27566.6^{+17448.6}_{-82.0}$	IH
SDSSJ103556.11+064143.9	$9.26^{+0.121}_{-0.035}$	$-2.106^{+0.202}_{-0.058}$	$3.131^{+0.3}_{-0.087}$	$87.9^{+12.0}_{-2.3}$	$2.2^{+4.7}_{-6.3}$	$-20.0^{+4.8}_{-0.2}$	$22.2^{+1.0}_{-1.0}$	$7.1^{+0.2}_{-0.1}$	$0.52^{+0.03}_{-0.01}$	$2137.3^{+60.4}_{-50.3}$	$-32395.0^{+1110.9}_{-1568.4}$	IH
	$12.915^{+0.102}_{-0.061}$	$-8.218^{+0.171}_{-0.102}$	$12.216^{+0.254}_{-0.346}$	$300.8^{+42.6}_{-25.2}$	$-60.8^{+43.7}_{-31.4}$	$25.1^{+11.4}_{-13.5}$	$147.8^{+25.5}_{-11.8}$	$11.9^{+0.4}_{-0.2}$	$0.86^{+0.02}_{-0.01}$	$-99.4^{+873.1}_{-641.6}$	$25522.1^{+5791.8}_{-2555.6}$	OH
SDSS J105519.28+232234.0	$9.313^{+0.197}_{-0.173}$	$-0.922^{+0.119}_{-0.136}$	$3.204^{+0.481}_{-0.421}$	$155.4^{+29.0}_{-25.8}$	$-150.7^{+19.3}_{-19.3}$	$90.2^{+8.6}_{-5.4}$	$15.2^{+2.7}_{-2.7}$	$4.9^{+0.4}_{-0.2}$	$0.52^{+0.04}_{-0.05}$	$790.4^{+169.0}_{-236.6}$	$-45745.3^{+4608.7}_{-4608.7}$	IH
SDSS J120441.38+120111.5	$8.213^{+0.021}_{-0.016}$	$-2.304^{+0.168}_{-0.228}$	$6.814^{+0.678}_{-0.499}$	$92.3^{+9.6}_{-9.1}$	$-149.9^{+10.1}_{-13.8}$	$6.2^{+4.3}_{-5.2}$	$12.8^{+0.7}_{-0.6}$	$3.7^{+0.3}_{-0.3}$	$0.55^{+0.04}_{-0.04}$	$597.9^{+110.1}_{-169.3}$	$-53841.3^{+1714.2}_{-1142.8}$	IH
SDSS J124719.46−034152.4	$6.874^{+0.081}_{-0.108}$	$-1.879^{+0.135}_{-0.18}$	$3.581^{+0.351}_{-0.263}$	$-141.4^{+15.7}_{-19.6}$	$-102.9^{+5.2}_{-10.4}$	$88.2^{+6.9}_{-5.6}$	$9.9^{+2.9}_{-0.0}$	$5.0^{+0.3}_{-0.2}$	$0.41^{+0.05}_{-0.05}$	$1263.5^{+31.8}_{-31.8}$	$-55819.2^{+2448.5}_{-2448.5}$	IH
	NB	NB	NB	NB	NB	NB	NB	NB	NB	NB	NB	NB
LAMOST J125346.09+075343.1	$7.856^{+0.006}_{-0.005}$	$-0.208^{+0.008}_{-0.008}$	$0.723^{+0.028}_{-0.027}$	$188.3^{+6.8}_{-6.8}$	$-148.3^{+4.7}_{-4.9}$	$2.6^{+2.6}_{-2.7}$	$13.4^{+0.4}_{-0.3}$	$1.9^{+0.1}_{-0.2}$	$0.75^{+0.03}_{-0.02}$	$766.8^{+40.7}_{-42.5}$	$-56611.4^{+914.8}_{-774.1}$	P
SDSS J131326.89−001941.4	$4.472^{+0.866}_{-1.126}$	$-3.561^{+0.874}_{-1.136}$	$9.327^{+3.014}_{-2.318}$	$92.1^{+7.3}_{-6.7}$	$-443.7^{+81.5}_{-124.4}$	$99.5^{+33.6}_{-43.7}$	$20.4^{+39.8}_{-8.5}$	$8.5^{+3.3}_{-1.6}$	$0.41^{+0.26}_{-0.13}$	$-1256.6^{+383.5}_{-264.5}$	$-34000.2^{+35769.3}_{-16692.3}$	IH
HE 1310−0536	$0.259^{+0.29}_{-0.29}$	$-8.32^{+0.311}_{-0.311}$	$17.184^{+0.644}_{-0.644}$	$-284.9^{+13.2}_{-12.5}$	$-448.9^{+16.8}_{-15.2}$	$47.0^{+3.4}_{-3.2}$	$99.7^{+38.3}_{-26.0}$	$19.0^{+0.7}_{-0.7}$	$0.68^{+0.06}_{-0.07}$	$2216.2^{+238.5}_{-238.5}$	$15227.9^{+8052.8}_{-8052.8}$	OH
HE 1327−2326	$7.332^{+0.028}_{-0.022}$	$-0.686^{+0.028}_{-0.023}$	$0.755^{+0.025}_{-0.031}$	$-279.3^{+12.7}_{-10.7}$	$-68.7^{+1.4}_{-1.3}$	$287.8^{+8.5}_{-10.6}$	$91.4^{+18.5}_{-17.0}$	$7.4^{+0.0}_{-0.0}$	$0.85^{+0.02}_{-0.03}$	$1522.3^{+4.9}_{-5.6}$	$11193.7^{+5154.1}_{-6091.2}$	OH
HE 1424−0241	$1.915^{+0.468}_{-0.54}$	$-1.738^{+0.134}_{-0.154}$	$8.108^{+0.723}_{-0.627}$	$-26.0^{+5.5}_{-7.0}$	$-233.7^{+16.1}_{-22.8}$	$44.9^{+2.2}_{-2.1}$	$8.8^{+0.7}_{-0.6}$	$0.9^{+0.5}_{-0.3}$	$0.81^{+0.06}_{-0.09}$	$58.6^{+38.9}_{-23.9}$	$-71087.9^{+2804.7}_{-1869.8}$	IH
SDSS J144256.37−001542.7	NB	NB	NB	NB	NB	NB	NB	NB	NB	NB	NB	NB
	$6.366^{+0.089}_{-0.221}$	$-0.233^{+0.013}_{-0.032}$	$2.033^{+0.283}_{-0.113}$	$93.2^{+6.6}_{-7.6}$	$42.0^{+8.0}_{-6.4}$	$217.1^{+9.0}_{-9.0}$	$39.1^{+5.2}_{-2.6}$	$6.7^{+0.1}_{-0.1}$	$0.71^{+0.03}_{-0.02}$	$1832.0^{+27.4}_{-18.2}$	$-14290.8^{+3324.2}_{-1662.1}$	OH
Pristine 221.8781+9.7844	$3.941^{+0.29}_{-0.38}$	$0.432^{+0.041}_{-0.031}$	$6.4^{+0.602}_{-0.46}$	$-249.6^{+12.4}_{-18.2}$	$-194.4^{+12.6}_{-19.9}$	$-6.7^{+12.7}_{-8.7}$	$14.1^{+2.3}_{-1.1}$	$4.9^{+0.7}_{-0.5}$	$0.49^{+0.01}_{-0.01}$	$123.6^{+83.8}_{-119.7}$	$-47818.2^{+5527.2}_{-3684.8}$	IH/S
SDSS J164234.48+443004.9	$7.283^{+0.048}_{-0.072}$	$1.869^{+0.196}_{-0.13}$	$1.742^{+0.182}_{-0.121}$	$-124.6^{+6.1}_{-9.1}$	$-143.0^{+4.5}_{-6.1}$	$-6.7^{+8.7}_{-5.8}$	$9.2^{+0.0}_{-0.0}$	$1.6^{+0.2}_{-0.2}$	$0.72^{+0.03}_{-0.04}$	$539.8^{+82.0}_{-41.0}$	$-70959.7^{+2586.2}_{-0.0}$	P
SDSS J173403.91+644633.0	$8.374^{+0.131}_{-0.058}$	$4.823^{+1.691}_{-0.752}$	$3.089^{+1.083}_{-0.481}$	$66.2^{+25.0}_{-16.7}$	$-174.4^{+20.0}_{-15.0}$	$-200.0^{+16.2}_{-23.1}$	$13.0^{+5.5}_{-2.7}$	$7.7^{+1.8}_{-1.3}$	$0.33^{+0.07}_{-0.06}$	$980.4^{+414.3}_{-207.1}$	$-43731.4^{+9796.3}_{-7347.2}$	IH
	NB	NB	NB	NB	NB	NB	NB	NB	NB	NB	NB	NB
SDSS J174259.67+253135.8	$5.293^{+0.294}_{-0.336}$	$3.185^{+0.399}_{-0.349}$	$2.0^{+0.25}_{-0.219}$	$74.6^{+26.6}_{-21.6}$	$-348.1^{+23.9}_{-27.3}$	$-58.7^{+8.8}_{-7.6}$	$8.0^{+1.3}_{-0.7}$	$1.0^{+0.2}_{-0.2}$	$0.77^{+0.06}_{-0.04}$	$-227.0^{+71.9}_{-61.6}$	$-78634.3^{+5992.5}_{-3424.3}$	IH/ω/P
	NB	NB	NB	NB	NB	NB	NB	NB	NB	NB	NB	NB
2MASS J18082002−5104378	$7.40^{+0.02}_{-0.03}$	$-0.189^{+0.007}_{-0.008}$	$-0.163^{+0.006}_{-0.007}$	$2.19^{+0.53}_{-0.53}$	$-45.4^{+1.6}_{-1.7}$	$-5.2^{+0.2}_{-0.2}$	$7.6^{+0.1}_{-0.1}$	$6.3^{+0.1}_{-0.1}$	$0.091^{+0.006}_{-0.005}$	$1520.0^{+17.0}_{-18.4}$	$-64227.3^{+509.0}_{-509.0}$	P
BPS CS 22891−0200	$-2.803^{+0.469}_{-0.469}$	$-5.036^{+0.219}_{-0.219}$	$-6.553^{+0.285}_{-0.285}$	$255.7^{+11.1}_{-11.1}$	$-93.4^{+4.6}_{-4.9}$	$222.1^{+14.0}_{-12.5}$	$64.0^{+18.9}_{-11.1}$	$7.4^{+0.6}_{-0.6}$	$0.8^{+0.03}_{-0.02}$	$-1788.2^{+160.3}_{-171.0}$	$1304.9^{+7251.3}_{-6445.6}$	OH
BPS CS 22885−0096	$2.413^{+0.302}_{-0.302}$	$0.123^{+0.007}_{-0.007}$	$-3.701^{+0.2}_{-0.2}$	$-145.0^{+8.6}_{-8.1}$	$-241.8^{+12.1}_{-12.9}$	$223.8^{+7.2}_{-7.2}$	$9.3^{+0.6}_{-1.3}$	$3.6^{+0.3}_{-0.3}$	$0.44^{+0.06}_{-0.06}$	$5.2^{+36.0}_{-29.7}$	$-63004.7^{+2672.9}_{-2672.9}$	IH/S
BPS CS 22950−0046	$-6.594^{+0.353}_{-0.243}$	$8.665^{+0.144}_{-0.21}$	$-8.233^{+0.199}_{-0.137}$	$59.4^{+8.2}_{-7.7}$	$-70.6^{+5.8}_{-5.5}$	$-222.9^{+6.8}_{-5.6}$	$41.7^{+3.6}_{-3.2}$	$2.5^{+0.4}_{-0.4}$	$0.89^{+0.02}_{-0.02}$	$-572.2^{+56.5}_{-56.5}$	$-14149.5^{+2904.8}_{-2582.0}$	OH
BPS CS 30336−0049	$-4.037^{+0.507}_{-0.475}$	$3.41^{+0.135}_{-0.144}$	$-9.176^{+0.386}_{-0.362}$	$-31.8^{+6.6}_{-6.6}$	$-643.6^{+25.2}_{-23.6}$	$119.8^{+1.9}_{-2.4}$	$122.7^{+51.1}_{-41.4}$	$8.1^{+0.8}_{-0.8}$	$0.88^{+0.03}_{-0.04}$	$1489.5^{+305.3}_{-305.3}$	$19080.8^{+11833.4}_{-11833.4}$	OH
HE 2139−5432	$0.746^{+0.54}_{-0.607}$	$-2.466^{+0.183}_{-0.206}$	$-8.023^{+0.597}_{-0.672}$	$-48.5^{+11.6}_{-12.3}$	$-264.7^{+18.4}_{-20.7}$	$-113.8^{+8.5}_{-8.5}$	$9.8^{+1.1}_{-0.9}$	$1.1^{+0.5}_{-0.3}$	$0.79^{+0.05}_{-0.06}$	$87.2^{+37.9}_{-27.1}$	$-66571.3^{+4078.3}_{-3625.1}$	IH

Table 4 – *continued*

Identifier	X (kpc)	Y (kpc)	Z (kpc)	U (km s^{-1})	V (km s^{-1})	W (km s^{-1})	Apo (kpc)	Peri (kpc)	ε	L$_Z$ (km s^{-1} kpc)	E (km^2 s^{-2})	Orbit
HE 2239−5019	$5.857^{+0.137}_{-0.142}$	$-0.731^{+0.047}_{-0.049}$	$-3.406^{+0.217}_{-0.226}$	$125.2^{+4.6}_{-4.6}$	$-540.5^{+29.3}_{-30.5}$	$-248.0^{+3.9}_{-3.7}$	$52.9^{+16.6}_{-10.4}$	$6.8^{+0.0}_{-0.0}$	$0.77^{+0.05}_{-0.05}$	$-1792.6^{+141.3}_{-141.3}$	$-4551.9^{+7794.6}_{-7145.0}$	OH
HE 2323−0256	$6.687^{+0.076}_{-0.053}$	$7.11^{+0.29}_{-0.411}$	$-11.698^{+0.674}_{-0.476}$	$-53.7^{+4.4}_{-5.3}$	$-199.4^{+8.4}_{-6.1}$	$20.4^{+5.7}_{-4.2}$	$15.4^{+0.5}_{-0.6}$	$2.8^{+0.2}_{-0.2}$	$0.68^{+0.03}_{-0.03}$	$44.7^{+94.9}_{-78.1}$	$-48598.2^{+1025.7}_{-1172.2}$	IH

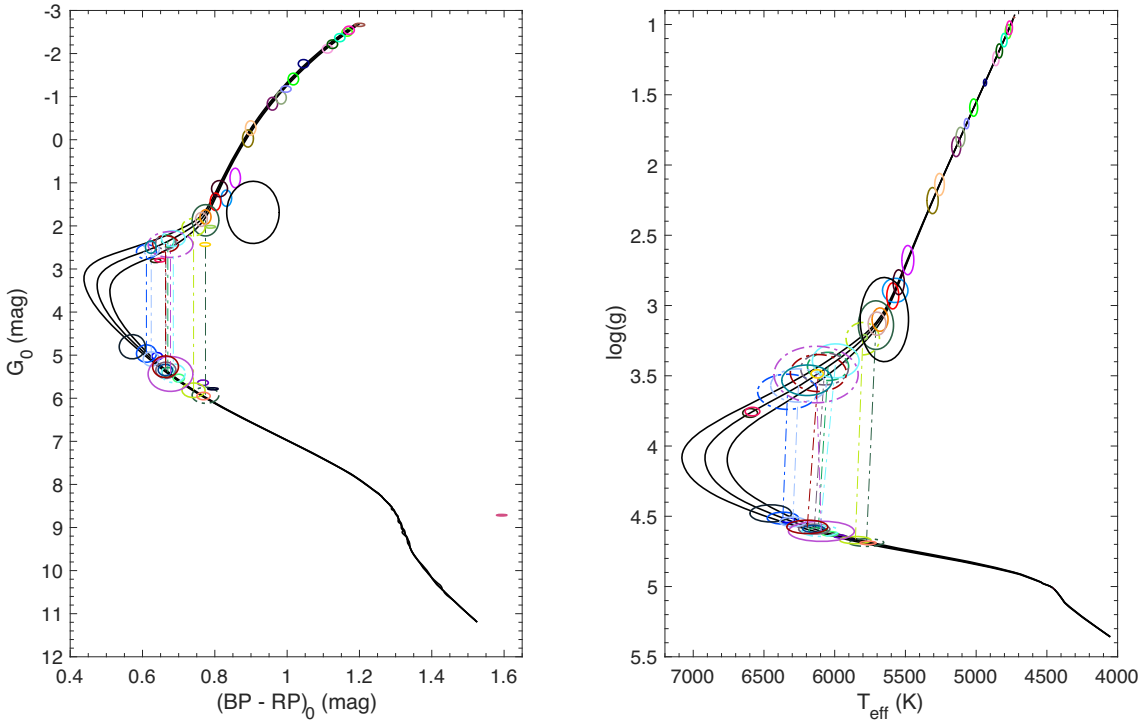

Figure 1. Position of the sample stars in the CMD (left) and the $\log(g)$ versus $T_{\rm eff}$ plane (right). The ellipses represent the position of the stars within 1σ and the black lines correspond to the three isochrones with $\log(A/{\rm yr}) = 10.05$, 10.10, 10.15 and metallicity [Fe/H] $= -4$ dex. If the dwarf-giant degeneracy is not broken, the two possible solutions are represented and connected by a dot–dashed line of the same colour code. Each colour represents a star and the colour-code is the same as the colour-code for the markers in Fig. 2 and the panel's titles in Figs A1–A42 (available Online). Solutions with integrated probability ($\int_{d-3\sigma}^{d+3\sigma} P(r){\rm d}r$) lower than 5 per cent are not shown and solutions with integrated probability in the range [5 per cent, 50 per cent] are shown with dot–dashed ellipses.

For all 42 stars in our sample, we show the results of our analysis in Figs A1–A42 (available Online). In all figures, the top-left panel shows the distance likelihood functions and posterior PDFs, the top-middle panel presents the log(g) PDF, while the top-right panel shows the effective temperature PDF. The orbit of the star in Galactic Cartesian coordinates is presented in the bottom panels of the figures.

In the subsections of Appendix A (available Online), we discuss in detail the results for every star in the sample sorted by right ascension. Specifically, we focus on the inferred distances, stellar parameters, and orbits using a MW halo prior and, when it yields different results, we also discuss the use of the disc+halo prior. A global comparison between the inferred stellar parameters form our work and the values from the literature is described in Appendix B (available Online) and shown in the two panels of Fig. B1.

We did a comparison between the distances inferred in this work and the ones inferred by Bailer-Jones et al. (2018). These authors use a posterior probability composed by the astrometric likelihood shown in equation (8) and a MW prior that is based on a Gaia-observed Galaxy distribution function accurately describing the overall distribution of all MW stars. This is naturally more biased to higher densities in the thin disc and thus results in closer distances for most of the stars.

Frebel et al. (2018) compiled a list of 29 UMP stars inferring orbital parameters starting from the MW prior described in Bailer-Jones et al. (2018), but fixing the length-scale parameter to $L = 0.5$. As both the initial assumptions and the focus of the analysis given in Frebel et al. (2018) significantly differ from the approach taken in this work, we refrain from a further qualitative comparison.

5 DISCUSSIONS

Our combined analysis of the *Gaia DR2* astrometry and photometry with stellar population models for low-metallicity stars allows us to infer the stellar parameters and orbital properties of the 42 known

UMP stars. We derive well constrained properties for most stars and, in particular, we are now in a position to unravel the possible origin of the heterogeneous sample of UMP stars found to date.

5.1 Insights on the orbits of UMP stars

Apart from two ambiguous cases, we can classify the orbits of the UMP stars within three loosely defined categories:

(i) 19 'inner halo' stars, arbitrarily defined as having apocentres smaller than 30 kpc.
(ii) 12 'outer halo' stars with apocentre larger than 30 kpc.
(iii) Strikingly, 11 stars that have 'MW plane' orbits, by which we mean that they stay confined close to the MW plane ($|Z| < 3.0$ kpc).

Fig. 2 attempts to show these different kind of orbits, displaying on the top panel the vertical component of the action-angle J_z versus the rotational component J_ϕ ($=L_z$) for all the UMP in our sample. In this space, the stars confined to the MW plane (denoted by a star marker) are constrained to the lower part of the diagram, while the halo stars have larger J_z. Stars that have a prograde motion have $J_\phi > 0$ and stars with retrograde orbits lie in the $J_\phi < 0$ part of the diagram. We note how the Caffau star (SDSS J102915+172927) and 2MASS J18082002−5104378 occupy a special place in this plane and they are the only stars on a quasi-circular orbit at large J_ϕ and low J_z.

It is appealing to assign a tentative origin to stars in these three categories. The 'inner halo' stars could well be stars accreted on to the MW during its youth, when its mass was smaller and therefore its potential well less deep than it is now. At that time, more energetic orbits would have been unbound and left the MW in formation. 'Outer halo' orbits tend to have very radial orbits in this sample (likely a consequence of the window function imparted by the various surveys that discovered these UMP stars; see below), which makes it easier to identify them. It is tempting to see those as being brought in through the accretion of faint dwarf galaxies on to the MW throughout the hierarchical formation of its halo. Although no UMP has been found in MW satellite dwarf galaxies yet, we know of many extremely metal-poor stars in these systems, down to [Fe/H] $= -4$ (e.g. Tafelmeyer et al. 2010) and UMP stars are expected to be present as well (Salvadori, Skúladóttir & Tolstoy 2015). We note that, among the two 'halo' categories, there is a distinct preference for prograde over retrograde orbits.

The 11 'MW plane' orbits are much more unexpected:

(i) 8 stars (SDSS J014036.21+234458.1, BD+44 493, HE 0233−0343, HE 0330+0148, HE 1012−1540, SDSS J103402.70+070116.6, LAMOST J125346.09+075343, SDSS J164234.48+443004.9) share similar rosette orbits within a wide range of angular momentum along the z axis ($83 \lesssim L_z \lesssim 885$ km s^{-1} kpc). These stars orbit close to the plane, but not on circular orbits.
(ii) SDSS J102915+172927 and 2MASS J18082002−5104378 (Figs A19 and A35 available Online), are on almost circular orbits close to the solar radius.
(iii) SDSS J174259.67+253135.8 (Fig. A34, available Online) is retrograde and more likely on an 'inner halo' orbit that remains close to the MW plane.

The first 10 of those stars, excluding SDSS J174259.67+253135.8, all have positive L_z and thus a prograde orbit, which is unlikely to be a random occurrence (< 1 per cent chance). It is worth noting that it is very unlikely the selection functions that led to the discovery of the UMP stars biased the sample for/against prograde orbit. The origin of those stars is puzzling but we can venture three different hypothesis for their presence in the sample, all of which must account for the fact that this significant fraction of UMP stars, which are expected to be very old, appears to know where the plane of the MW is located, even though the MW plane was unlikely to be in place when they formed.

Scenario 1: The first obvious scenario is that these stars formed in the MW disc itself after the HI disc settled. In this fashion, the stars were born with a quasi-circular orbit and then the presence of a dynamical heating mechanism is mandatory to increase the eccentricity and the height from the plane as a function of time. We find that all the prograde 'MW plane' stars and few catalogued as inner halo stars that are confined within $Z_{\rm max} < 15$ kpc and $d_{\rm apo} < 25$ kpc (see Fig. 2) overlap in the parameters space ($Z_{\rm max}$, $d_{\rm apo}$, L_z, E) with a population of known stars at higher metallicity that Haywood et al. (2018) hypothesize to be born in the thick disc and then dynamical heated by the interaction between the disc and a merging satellite. However, the question is whether in a relatively well-mixed HI disc it is possible to form stars so completely devoid of metals.

Scenario 2: The second scenario is that these stars were brought into the MW by the accretion of a massive satellite dwarf galaxy. Cosmological simulations have shown that merger events are expected to sometimes be aligned with the disc. As a result, significant stellar populations currently in the disc might actually be merger debris (Gómez et al. 2017). Alternatively, Scannapieco et al. (2011), show that 5–20 per cent of disc stars in their simulated MW-like disc galaxies were not formed *in situ* but, instead, accreted early from now disrupted satellites on co-planar orbits. Additionally, it is well known that the accretion of a massive system on to the MW will see its orbit align with the plane of the MW via dynamical friction, as shown by Peñarrubia, Kroupa & Boily (2002) or Abadi et al. (2003). From these authors' simulations, one would expect orbits to become such that they would end up with larger eccentricities than the satellite's orbit at the start of the merging process and also aligned with the disc by dynamical friction and tidal interactions, which is compatible with our orbital inference for the remarkable UMP stars. If such an accretion took place in the MW's past, it could have brought with it a significant fraction of the UMP stars discovered in the solar neighbourhood. The accretion of the so-called Gaia-Enceladus satellite in the Milky Way's past (Belokurov et al. 2018; Haywood et al. 2018; Helmi et al. 2018) could be an obvious culprit, however Gaia-Enceladus was discovered via the mainly halo-like and retrograde orbit of its stars whereas the vast majority of the stars we find here are on prograde orbits. In fact, there is no evidence of a particular overdensity of stars in the top-left region of the J_z versus J_ϕ of Fig. 2 where Gaia-Enceladus stars are expected to be found. It would therefore be necessary to summon the presence of another massive or several less massive accretion events on to the MW if this scenario is valid.

Scenario 3: Finally, the third scenario that could explain the presence of this significant fraction of UMP stars that remain confined to the plane of the MW would be one in which these stars originally belonged to one or more of the building blocks of the proto-MW, as it was assembling into the MW that we know today. Fully cosmological simulations confirm that stars that are at the present time deeply embedded in our Galaxy do not need to have their origin in the proto-Galaxy. El-Badry et al. (2018) find in their cosmological simulations that of all stars formed before $z = 5$ presently within 10 kpc of the Galactic centre less than half were already in the main progenitor at $z = 5$. Over half of these extremely

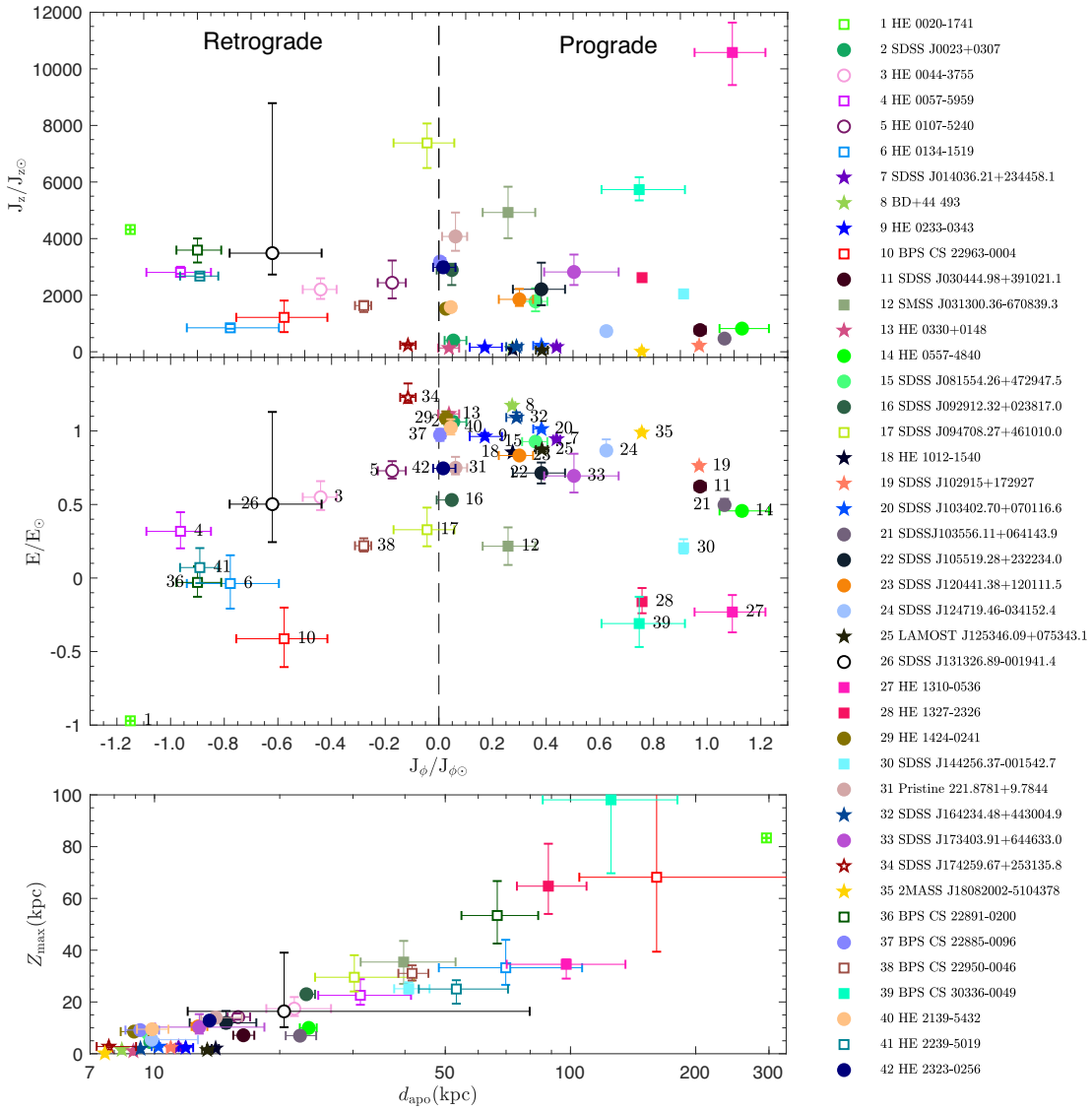

Figure 2. Position of the sample stars in the rotational action J_ϕ ($=L_z$) and vertical action J_z space (top panel), in the energy and rotational action space, and in the maximum height versus apocentre of the stars' orbits (bottom panel). The rotational and vertical action and the Energy are scaled by the Sun values respectively $J_{\phi\odot} = 2009.92\,\mathrm{km\ s^{-1}\ kpc}$, $J_{z\odot} = 0.35\,\mathrm{km\ s^{-1}\ kpc}$, and $E_\odot = -64943.61\,\mathrm{km^2\ s^{-2}}$. Stars within our 'MW planar' sample that are confined close to the MW plane are marked with a star symbols, while 'inner halo' and 'outer halo' stars are represented by circles and squares, respectively. Retrograde stars, which are located on the left side of the top and central panels ($J_\phi < 0\,\mathrm{km\ s^{-1}\ kpc}$) are denoted with empty marker, while prograde stars are shown with a filled marked. The colour-coding is the same as in Fig. 1 and as the title of Figs A1–A42 (available Online) and helps to differentiate the stars. The full legend is provided on the side of this figure. The number associated to each star also corresponds to the number of the subsection in the Appendix A (available Online) in which the individual results are discussed.

old stars would thus make their way into the main Galaxy in later merging events and find themselves at $z = 5$ inside different building blocks that are up to 300 kpc away from the main progenitor centre. In such a scenario, we can expect that whatever gas-rich blocks formed the backbone of the MW disc brought with it its own stars, including UMP stars. Yet, for such a significant number of UMP stars to align with the current MW plane, it is necessary to assume that the formation of the MW's disc involved a single massive event that imprinted the disc plane that is aligned with the orbit of its stars. The presence of many massive building blocks would have likely led to changes in the angular HI disc alignment. Similarly, the MW cannot have suffered many massive accretions since high redshift or the disc would have changed its orientation (Scannapieco et al. 2009). This would be in line with expectations that the MW has had an (unusually) quiet accretion history throughout its life (Wyse 2001; Stewart et al. 2008).

5.1.1 *The Caffau star and 2MASS J18082002−5104378*

SDSS J102915+172927 (see Fig. A19, available Online), also known as 'the Caffau star' (Caffau et al. 2011), and 2MASS J18082002−5104378 (see Fig. A35, available Online) both have a disc-like prograde orbit but while the Caffau Star reaches a height of 2.3 kpc from the MW plane, the latter star is

confined within 0.166 kpc, confirming the results from Schlaufman, Thompson & Casey (2018). Both stars represent outliers inside the surprising sample of 'MW planar' stars that typically have more eccentric orbits. For these stars, scenario 3, as outlined above, might be an interesting possibility. A merging between the building blocks of the proto-MW could have brought in these UMP stars and their orbit circularized by dynamical friction.

5.1.2 Coincidence with the Sagittarius stream

We note that four of the 'halo' stars (SDSS J092912.32+023817.0, SDSS J094708.27+461010.0, Pristine221.8781+9.7844 and BPS CS 22885−0096) have orbits that are almost perpendicular to the MW plane (see Figs A16, A17, A31, and A37 available Online), coinciding with the plane of the stellar stream left by the Sagittarius (Sgr) dwarf galaxy as it as being tidally disrupted by the MW. We therefore investigate if these stars belong to the stream by comparing their proper motions and distances with the values provided by the N-body simulation of Law & Majewski (2010) (hereafter LM10; Fig. 3). It is clear that SDSS J094708.27+461010.0 has a proper motion that is incompatible with the simulation's particles. On the other hand, we find that SDSS J092912.32+023817.0, Pristine221.8781+9.7844, and BPS CS 22885−0096 have proper motions that are in broad agreement with those of the simulation. These stars could be compatible with the oldest wraps of the Sgr galaxy but we are nevertheless cautious in this assignment since only the young wraps of the stream were constrained well with observations in the Law & Majewski (2010) model. Older wraps rely on the simulation's capability to trace the orbit back in the MW potential that is itself poorly constrained and has likely changed over these time-scales, and the true 6D phase-space location the older warps could therefore easily deviate significantly from the simulation's expectations.

5.1.3 A connection between SDSS J174259.67+253135.8 and ω Centauri?

SDSS J174259.67+253135.8 is the only star of the 'MW planar' sample that has a retrograde motion and its orbital properties are, in fact, similar enough to those of the ω Centauri (ωCen) stellar cluster to hint at a possible connection between the two. It should be noted, however, that the L_z of ωCen's orbit is about twice that of this star. Nevertheless, given the dynamically active life that ωCen must have had in the commonly-held scenario that it is the nucleus of a dwarf galaxy accreted by the Milky Way long ago (e.g. Zinnecker et al. 1988; Mizutani, Chiba & Sakamoto 2003), the similarity of the orbits is intriguing enough to warrant further inspection.

5.2 Limits of the analysis and completeness

The heterogeneous UMP sample comes from multiple surveys conducted over the years, with their own, different window functions for the selection of the targets and it can thus by no means be called a complete or homogeneous sample. To reconstruct the full selection function of this sample is nearly impossible since it includes so many inherited window functions from various surveys and follow-up programs. As far as we can deduce, however, none of the programs would have specifically selected stars on particular orbits. We therefore consider the clear preference of the UMP star population for orbits in the plane of the MW disc a strong result of this work but we caution the reader not to consider the ratio of 'inner halo,' 'outer halo,' and 'MW plane' orbits as necessarily representative of the true ratios, which will require a more systematic survey to confirm.

We note that due to the different abundance patterns of these stars, [Fe/H] is not always a good tracer of the total metallicity [M/H]. However, not all stars in this sample are equally well-studied and therefore constraints on [M/H] are inhomogeneous. This has led us to nevertheless choose a cut on [Fe/H] as this is the common quantity measured by all the cited authors.

Another limitation of this work comes from the isochrones we use, which are the most metal-poor isochrones available in the literature at this time and have [Fe/H] = −4 dex with solar-scaled α-abundances. Beyond the fact that some stars in our sample are significantly more metal-poor than this, not all stars follow this abundance pattern and as a result their total metal-content can change, in turn affecting the colour of the isochrones. We estimate, however, that this will be a small effect at these low metallicities, as low-metallicity isochrones are relatively insensitive to small variations in metallicity, and take this into account adding a systematic uncertainty of 0.01 mag in quadrature to the model (see Section 3.1.1). This is unlikely to affect the final results on the evolutionary phase and the typology of the orbits. A final potential limitation of this work stems from the possible binary of some of the studied stars. If, unbeknownst to us, a star is in fact a binary system whose component are in the same or a similar evolutionary phase, their photometry would not be representative of their true properties and our distance inference would be biased. Similarly a binary star would like have its velocity be affected, leading to flawed orbital parameters. For known binary stars, we nevertheless take these effects into account and our distance and orbital inference should not be severely affected by this binarity issue.

5.3 Future outlook

As described in 5.2, the current sample and analysis of their dynamics is quite limited by an unknown and complicated selection function. With proper motion, parallax, and the exquisite photometry from *Gaia DR2*, we plan to apply the same bayesian framework described in Section 3 to all the EMP stars within the Pristine survey (Starkenburg et al. 2017a) to investigate their stellar properties and orbits. As the completeness and purity of this sample is very well understood (Youakim et al. 2017) and this sample is much larger, this will open up more quantitative avenues to explore the role of extremely metal-poor stars in the big picture of the accretion history of the MW.

6 CONCLUSIONS

Combining the *Gaia DR2* photometric and astrometric information in a statistical framework, we determine the posterior probability distribution function for the distance, the stellar parameters (temperature and surface gravity), and the orbital parameters of 42 UMPs (see Tables 3 and 4). Given that 11 of those stars remain confined close to the MW plane, we use both a pure halo prior and a combined disc+halo prior. Folding together distance posterior and orbital analysis we find that 18 stars are on the main sequence and the other 24 stars are in a more evolved phase (subgiant or giant).

Through the orbital analysis, we find that 11 stars are orbiting close to the plane of the disc, with maximum height above the disc within 3 kpc. We hypothesize that they could have once belonged to a massive building block of the proto-MW that formed the backbone of the MW disc, or that they were brought into

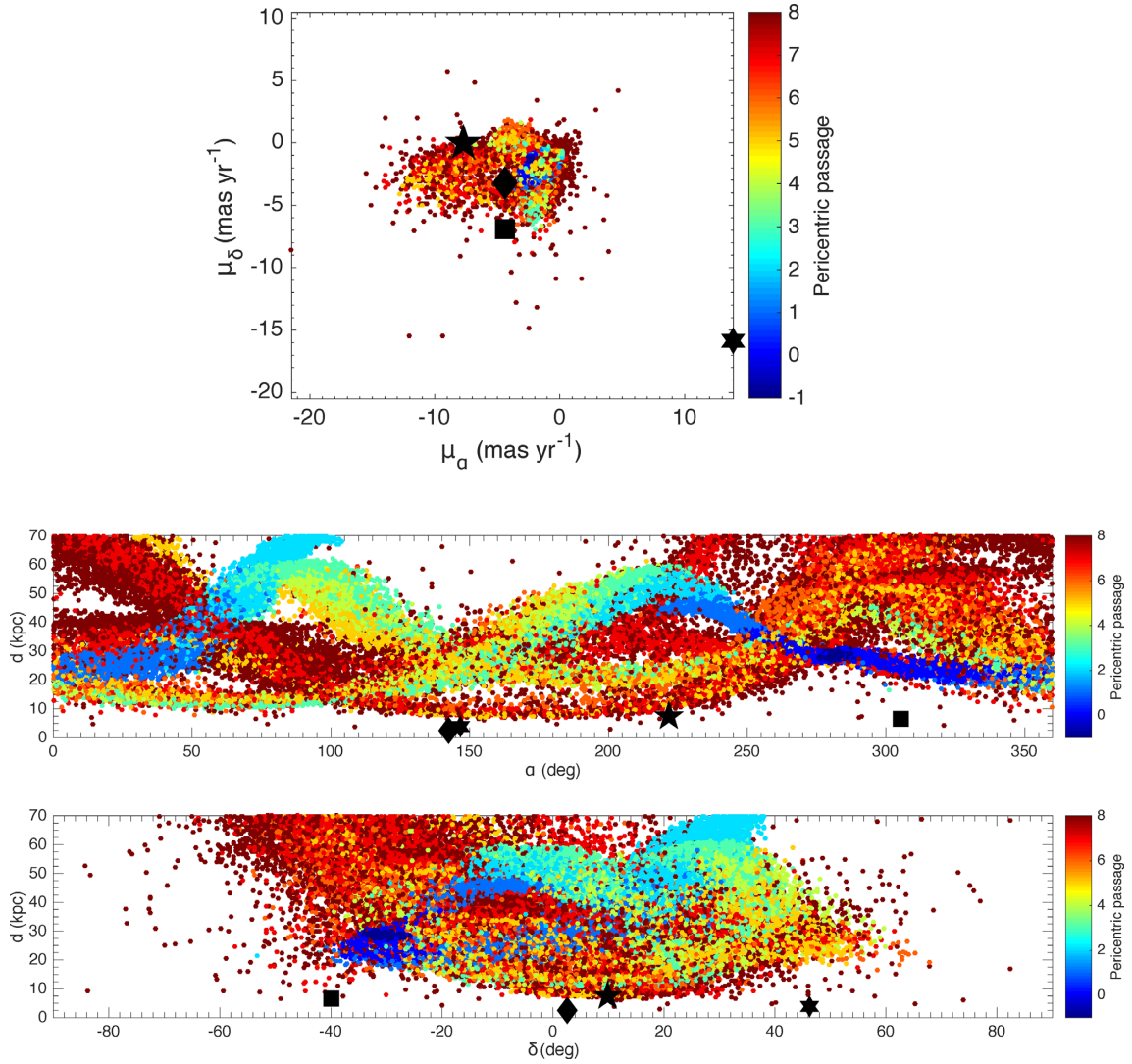

Figure 3. Top: proper motion space for the particles of the LM10 simulation (dots), and SDSS J092912.32+023817.0 (black diamond), SDSS J094708.27+461010.0 (black hexagram), Pristine221.8781+9.7844 (black pentagram), and BPS CS 22885−0096 (black square). The colour-code for the LM10 simulation indicates the pericentric passage on which the particle became unbound from Sgr. A pericentric passage value of −1 indicates debris which is still bound at the present day, while a value of 0 indicates debris stripped on the most recent pericentric passage of Sgr, and a value above 1 corresponds to successive pericentric passages. Centre: heliocentric distance d as a function of right ascension α for the LM10 simulation and the candidates. Bottom: heliocentric distance d as a function of declination δ for the LM10 simulation and the candidates. The LM10 simulation is shown within 70 kpc from the Sun for the centre and bottom panel.

the MW via a specific, massive hierarchical accretion event, or they might have formed in the early disc and have been dynamically heated. Another 31 stars are from both the 'inner halo' (arbitrarily defined as having $r_{\rm apo} < 30$ kpc) and were accreted early on in the history of the MW, or the 'outer halo' hinting that they were accreted on to the Galaxy from now-defunct dwarf galaxies. Of these halo stars, SDSS J092912.32+023817.0, Pristine221.8781+9.7844, and BPS CS 22885−0096, could possibly be associated with the Sagittarius stream, although they would need to have been stripped during old pericentric passages of the dwarf galaxy. SDSS J174259.67+253135.8 could also possibly be associated with ωCen as its progenitor.

The work presented here provides distances, stellar parameters, and orbits for all known UMP stars and, hence, some of the oldest stars known. To understand their position and kinematics within the Galaxy it is very important to reconstruct the early formation of the MW and/or the hierarchical formation of some of its components. We foresee a statistical improvement of this first study with the arrival of homogeneous and large data sets of EMP stars, such as observed within the Pristine or SkyMapper surveys (Starkenburg et al. 2017a; Wolf et al. 2018). With these surveys, the window function and the selection criteria of the objects for which distances and orbits are derived will be much better known.

ACKNOWLEDGEMENTS

We would like to thank Benoit Famaey, Misha Haywood, and Paola Di Matteo for the insightful discussions and comments.

FS, NFM, NL, and RI gratefully acknowledge funding from CNRS/INSU through the Programme National Galaxies et Cos-

mologie and through the CNRS grant PICS07708. FS thanks the Initiative dExcellence IdEx from the University of Strasbourg and the Programme Doctoral International PDI for funding his PhD. This work has been published under the framework of the IdEx Unistra and benefits from a funding from the state managed by the French National Research Agency as part of the investments for the future program. ES and AA gratefully acknowledge funding by the Emmy Noether program from the Deutsche Forschungsgemeinschaft (DFG). JIGH acknowledges financial support from the Spanish Ministry project MINECO AYA2017-86389-P, and from the Spanish MINECO under the 2013 Ramón y Cajal program MINECO RYC-2013-14875. KAV thanks NSERC for research funding through the Discovery Grants program.

This research has made use of use of the SIMBAD data base, operated at CDS, Strasbourg, France (Wenger et al. 2000). This work has made use of data from the European Space Agency (ESA) mission *Gaia* (https://www.cosmos.esa.int/gaia), processed by the *Gaia* Data Processing and Analysis Consortium (DPAC, https://www.cosmos.esa.int/web/gaia/dpac/consortium). Funding for the DPAC has been provided by national institutions, in particular the institutions participating in the *Gaia* Multilateral Agreement.

REFERENCES

Abadi M. G., Navarro J. F., Steinmetz M., Eke V. R., 2003, ApJ, 597, 21
Abohalima A., , Frebel A., 2018, ApJs, 238, 36
Aguado D. S., Allende Prieto C., González Hernández J. I., Carrera R., Rebolo R., Shetrone M., Lambert D. L., Fernández-Alvar E., 2016, A&A, 593, 13
Aguado D. S., Allende Prieto C., González Hernández J. I., Rebolo R., Caffau E., 2017a, A&A, 604, 7
Aguado D. S., González Hernández J. I., Allende Prieto C., Rebolo R., 2017b, A&A, 605, 10
Aguado D. S., González Hernández J. I., Allende Prieto C., Rebolo R., 2018b, ApJ, 852, 6
Aguado D. S., Allende Prieto C., González Hernández J. I., Rebolo R., 2018a, ApJ, 854, 4
Allende Prieto C. et al., 2015, A&A, 579, 6
Arentsen A., Starkenburg E., Shetrone M. D., Venn K. A., Depagne É., McConnachie A. W., 2019, A&A, 621, A108
Bailer-Jones C. A. L., Rybizki J., Fouesneau M., Mantelet G., Andrae R., 2018, AJ, 156, 58
Bailer-Jones C. A. L., 2015, PASP, 127, 994
Beers T. C., Christlieb N., 2005, ARA&A, 43, 531
Beers T. C., Preston G. W., Shectman S. A., 1985, AJ, 90, 2089
Belokurov V., Erkal D., Evans N. W., Koposov S. E., Deason A. J., 2018, MNRAS, 478, 611
Binney J., Tremaine S., 2008, Galactic Dynamics, 2nd edn. Princeton Univ. Press, Princeton
Bland-Hawthorn J., Gerhard O., 2016, ARA&A, 54, 529
Bonifacio P. et al., 2015, A&A, 579, 20
Bonifacio P. et al., 2018, A&A, 612, 10
Bovy J., 2015, ApJS, 216, 29
Caffau E. et al., 2011, Nature, 477, 67
Caffau E. et al., 2013a, A&A, 560, 7
Caffau E. et al., 2013b, A&A, 560, 9
Caffau E. et al., 2016, A&A, 595, 6
Cayrel R. et al., 2004, A&A, 416, 1117
Choi J., Dotter A., Conroy C., Cantiello M., Paxton B., Johnson B. D., 2016, ApJ, 823, 102
Christlieb N., Wisotzki L., Graßhoff G., 2002, A&A, 391, 397
Christlieb N., Gustafsson B., Korn A. J., Barklem P. S., Beers T. C., Bessell M. S., Karlsson T., Mizuno-Wiedner M., 2004, ApJ, 603, 708
Cohen J. G., Christlieb N., McWilliam A., Shectman S., Thompson I., Melendez J., Wisotzki L., Reimers D., 2008, ApJ, 672, 320
Cui X.-Q. et al., 2012, Res. Astron. Astrophys., 12, 1197
Dotter A., 2016, ApJS, 222, 8
Eisenstein D. J. et al., 2011, AJ, 142, 24
El-Badry K. et al., 2018, MNRAS, 480, 652
Evans D. W. et al., 2018, A&A, 616, 21
Frebel A., Norris J. E., 2015, ARA&A, 53, 631
Frebel A., Collet R., Eriksson K., Christlieb N., Aoki W., 2008, ApJ, 684, 588
Frebel A., Chiti A., Ji A. P., Jacobson H. R., Placco V. M., 2015, ApJ, 810, 7
Frebel A., Ji A. P., Ezzeddine R., Hansen T. T., Chiti A., Thompson I. B., Merle T., 2018, preprint (arXiv:1810.01228)
Freeman K., Bland-Hawthorn J., 2002, ARA&A, 40, 487
Gaia Collaboration, 2016, A&A, 595, 36
Gaia Collaboration, 2018, A&A, 616, A1
Gómez F. A. et al., 2017, MNRAS, 472, 3722
Greif T. H., 2015, Comput. Astrophys. Cosmol., 2, 36
Hansen T. et al., 2015, ApJ, 807, 17
Haywood M., Di Matteo P., Lehnert M. D., Snaith O., Khoperskov S., Gómez A., 2018, ApJ, 863, 113
Helmi A., , Babusiaux C., Koppelman H. H., Massari D., Veljanoski J., Brown A. G. A., 2018, Nature, 563, 85
Hernitschek N. et al., 2018, ApJ, 859, 32
Ito H., Aoki W., Beers T. C., Tominaga N., Honda S., Carollo D., 2013, ApJ, 773, 33
Karlsson T., Bromm V., Bland-Hawthorn J., 2013, Rev. Mod. Phys., 85, 809
Keller S. C. et al., 2014, Nature, 506, 463
Lai D. K., Bolte M., Johnson J. A., Lucatello S., Heger A., Woosley S. E., 2008, ApJ, 681, 1524
Law D. R., Majewski S. R., 2010, ApJ, 714, 229
Li H., Aoki W., Zhao G., Honda S., Christlieb N., Suda T., 2015, PASJ, 67, 84
Lindegren L. et al., 2018, A&A, 616, A2
Marigo P., Girardi L., Bressan A., Groenewegen M. A. T., Silva L., Granato G. L., 2008, A&A, 482, 883
Meléndez J., Placco V. M., Tucci-Maia M., Ramírez I., Li T. S., Perez G., 2016, A&A, 585, 5
Mizutani A., Chiba M., Sakamoto T., 2003, ApJ, 589, L89
Navarro J. F., Frenk C. S., White S. D. M., 1997, ApJ, 490, 493
Nordlander T., Amarsi A. M., Lind K., Asplund M., Barklem P. S., Casey A. R., Collet R., Leenaarts J., 2017, A&A, 597, 16
Norris J. E. et al., 2013, ApJ, 762, 16
Norris J. E., Christlieb N., Korn A. J., Eriksson K., Bessell M. S., Beers T. C., Wisotzki L., Reimers D., 2007, ApJ, 670, 774
Paxton B., Bildsten L., Dotter A., Herwig F., Lesaffre P., Timmes F., 2011, ApJS, 192, 3
Peñarrubia J., Kroupa P., Boily C. M., 2002, MNRAS, 333, 779
Placco V. M. et al., 2016, ApJ, 833, 13
Placco V. M., Frebel A., Lee Y. S., Jacobson H. R., Beers T. C., Pena J. M., Chan C., Heger A., 2015, ApJ, 809, 136
Plez B., Cohen J., Meléndez J., 2005, Hill V., Francois P., Primas F., Proceedings of The International Astronomical Union. p. 228
Roederer I. U., Preston G. W., Thompson I. B., Shectman S. A., Sneden C., Burley G. S., Kelson D. D., 2014, AJ, 147, 136
Salpeter E. E., 1955, ApJ, 121, 161
Salvadori S., Skúladóttir Á., Tolstoy E., 2015, MNRAS, 454, 1320
Scannapieco C., White S. D. M., Springel V., Tissera P. B., 2009, MNRAS, 396, 696
Scannapieco C., White S. D. M., Springel V., Tissera P. B., 2011, MNRAS, 417, 154
Schlaufman K. C., Thompson I. B., Casey A. R., 2018, ApJ, 867, 98
Schlegel D. J., Finkbeiner D. P., Davis M., 1998, ApJ, 500, 525
Schönrich R., Binney J., Dehnen W., 2010, MNRAS, 403, 1829
Sharma S., 2017, ARA&A, 55, 213
Starkenburg E. et al., 2017a, MNRAS, 471, 2587
Starkenburg E. et al., 2018, MNRAS, 481, 3838

Starkenburg E., Oman K. A., Navarro J. F., Crain R. A., Fattahi A., Frenk C. S., Sawala T., Schaye J., 2017b, MNRAS, 465, 2212
Stewart K. R., Bullock J. S., Wechsler R. H., Maller A. H., Zentner A. R., 2008, ApJ, 683, 597
Tafelmeyer M. et al., 2010, A&A, 524, 21
Wenger M. et al., 2000, A&AS, 143, 9
Wolf C. et al., 2018, PASA, 35, 29
Wyse R. F. G., 2001, in Funes J. G., Corsini E. M., eds, ASP Conf. Ser., Vol. 230, Galaxy Disks and Disk Galaxies. Astron. Soc. Pac., San Francisco, p. 71
Yanny B. et al., 2009, AJ, 137, 4377
Yong D. et al., 2013, ApJ, 762, 49
York D. G. et al., 2000, AJ, 120, 1579
Youakim K. et al., 2017, MNRAS, 472, 2963
Zinnecker H., Keable C. J., Dunlop J. S., Cannon R. D., Griffiths W. K., 1988, in Grindlay J. E., Philip A. G. D., eds, IAU Symposium, Vol. 126, The Harlow-Shapley Symposium on Globular Cluster Systems in Galaxies. Kluwer Academic Publishers, Dordrecht, p. 603

SUPPORTING INFORMATION

Supplementary data are available at *MNRAS* online.

Appendix A. Individual results.
Appendix B. Comparison with values from the literature.

Please note: Oxford University Press is not responsible for the content or functionality of any supporting materials supplied by the authors. Any queries (other than missing material) should be directed to the corresponding author for the article.

This paper has been typeset from a TEX/LATEX file prepared by the author.